CNIC-01140
CNDC-0019
INDC(CPR)-041/L

中国核科技报告

CHINA NUCLEAR SCIENCE AND TECHNOLOGY REPORT

COMMUNICATION OF NUCLEAR DATA PROGRESS

No. 16(1996)

China Nuclear Data Center

中国核情报中心
原子能出版社

China Nuclear Information Centre
Atomic Energy Press

CNIC-01140
CNDC-0019
INDC(CPR)-041 / L

COMMUNICATION OF NUCLEAR DATA PROGRESS

No. 16 (1996)

China Nuclear Data Center

China Nuclear Information Centre

Atomic Energy Press

Beijing, December, 1996

EDITORIAL NOTE

This is the 16th issue of *Communication of Nuclear Data Progress* (CNDP), in which the achievements in nuclear data field for the last year in P. R. China and a paper from India are carried. It includes the measurements of neutron activation cross section for $^{193}Ir(n,2n)^{192m2}Ir$ reaction at 14.7 MeV and fragment angular distributions in the fission of ^{197}Au, ^{207}Pb and ^{209}Bi induced by alpha particles up to 70 MeV; discrete level effect on spectrum calculations of secondary particles, calculations of $n+^{235}U$ ($E_n = 5$ MeV) scattering angle distribution by ECIS95 and various cross sections for $n+^{169}Tm$ and ^{103}Rh reactions up to 100 MeV and 25 MeV respectively, and $p+^{52}Cr$ reactions up to 30 MeV; evaluations of H total neutron cross section from 20 MeV to 2 GeV and $^{169}Tm(n,xn)^{168,\ 167,\ 166,\ 165}Tm$ reactions from threshold to 100 MeV, evaluation and calculation of production cross sections for ^{11}C, ^{13}N and ^{15}O medical radioisotopes from ^{11}B, ^{13}C, $^{15}N(p,n)$ and $^{16}O(p,x)^{13}N$ reactions up to 80 MeV; an approach of a systematic description of gamma–ray spectra from $(n,x\gamma)$ reactions induced by fast neutron; data files of optical model parameter and level density sub–libraries.

We hope that our readers and colleagues will not spare their comments, in order to improve the publication.

Please write to Drs. Liu Tingjin and Zhuang Youxiang
Mailing Address : China Nuclear Data Center
China Institute of Atomic Energy
P. O. Box 275 (41), Beijing 102413
People's Republic of China
Telephone : 86–10–69357729 or 69357830
Telex : 222373 IAE CN
Facsimile : 86–10–6935 7008
E–mail : CNDC@ MIPSA. CIAE. AC. CN

CONTENTS

CN9701135

I EXPERIMENTAL MEASUREMENT

A Tritium Gas Target for Neutron Production at HI−13 Tandem Accelerator

Qi Bujia Zhou Zuying Zhou Chenwei Tang Hongqing
Du Yanfeng Chen Qingwang Li Jimin

(China Institute of Atomic Energy, P. O. Box 275 (46), Beijing)

Abstract

A tritium gas target has been built and employed in neutron physics experiments at HI−13 tandem accelerator. The gas target consists of a helium gas cell and a tritium gas cell whose entrance windows are made of 10 μm thick molybdenum foil. The gas target is intended as a neutron source using $T(d,n)^4He$ and $T(p,n)^3He$ reactions. Details of the target design and performance are given.

A tritium gas target has been built and employed in neutron physics experiments at HI−13 tandem accelerator with both DC and pulsed beams. The neutron yields of the tritium gas target using the T(p,n) and T(d,n) reactions are higher than the ones of solid target under the same beam currents, meanwhile the target backgrounds can be reasonably measured. This target has been used in our time−of−flight neutron spectrometer to effectively carry out studies of elastic and inelastic neutron scattering and neutron induced charged particle emission reactions in the energy range up to 40 MeV. The gas target consists of a helium gas cell and a tritium gas cell. There is a flange at one end of the helium gas cell to which the entrance window is attached. The window between two gas cells is similar to the entrance one. The other end of the tritium gas cell is closed and its gas cell is lined by 0.3 mm thick gold plate and 1 mm thick gold disk serves as the beam stop. Gold has been shown to yield low neutron backgrounds when bombarded by charged particle. The Tritium cell is 4 cm long

with 0.3 mm thick and 1.1 cm in diameter, whose body is made of stainless steel. The cells in which O–rings and Indium O–ring are employed to accomplish entrance–foil attachment. A 80 cm long copper tube with 2.0 mm O. D. by 1.0 mm I. D. is silver–soldered into the cell flange to provide the connection with the gas handling system. Cross section view of the tritium gas target is shown in Fig. 1. The gas cell was cooled by water drops. The whole tritium loop was vacuum pressure and helium leak tested before being filled with tritium gas. The cell contained 2 atm. of tritium gas and other 0.2 atm. of helium gas. The gas pressure in cells are measured by pressure transducer, from which the signals through a dc amplifier come to a electronic module with alarm setting in the tandem accelerator control room. If the pressure of one of cells changes out of pressure range setting, it will send a signal to the fast valve which is about 15 meters from the cell in the beam tube and the fast valve will be closed automatically. The handling system diagram of the tritium gas target assembly is shown in Fig. 2. The whole handling system of the target system was enclosed in a glove box connected with a φ420 mm ventilating pipe system. While the target is used, the experimental area is monitored with a tritium air monitor. Bombarded onto the tritium gas cell with 20 MeV pulsed deuteron beam of an intensity of 1.5 μA, the gas target is reliable and the windows didn't show any sign of damage after 200 h of irradiation. The neutron TOF spectra of $T(p,n)^3He$ and $T(d,n)^4He$ reaction at $E_p = 7$ MeV and $E_d = 20$ MeV are shown in Fig. 3. As neutron source using $T(d,n)^4He$ reaction, elastic scattering differential cross sections at 37 MeV for ^{209}Bi and C have been measured at 42 Lab. angles (11° to 140°). As neutron source using $T(p,n)^3He$ reaction, prompt neutron spectra of ^{238}U fission induced by 5.4 MeV neutrons have been measured. The performance of the gas target is very satisfactory in neutron physics experiments at HI–13 tandem accelerator.

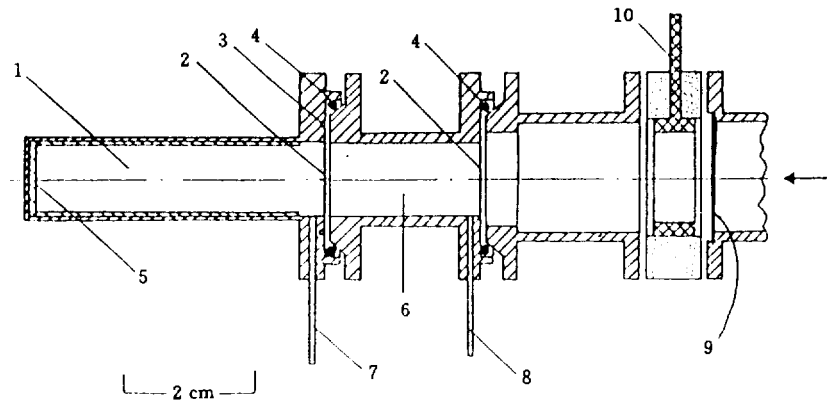

Fig. 1 Cross section view of the tritium gas target

1. Tritium gas cell; 2. Mo foil; 3. Indium O–ring; 4. O–ring;
5. Au beam stop; 6. Helium gas cell; 7. Tritium gas filling tube;
8. Helium gas filling tube; 9. Ta collimator; 10. Electron suppressor ring.

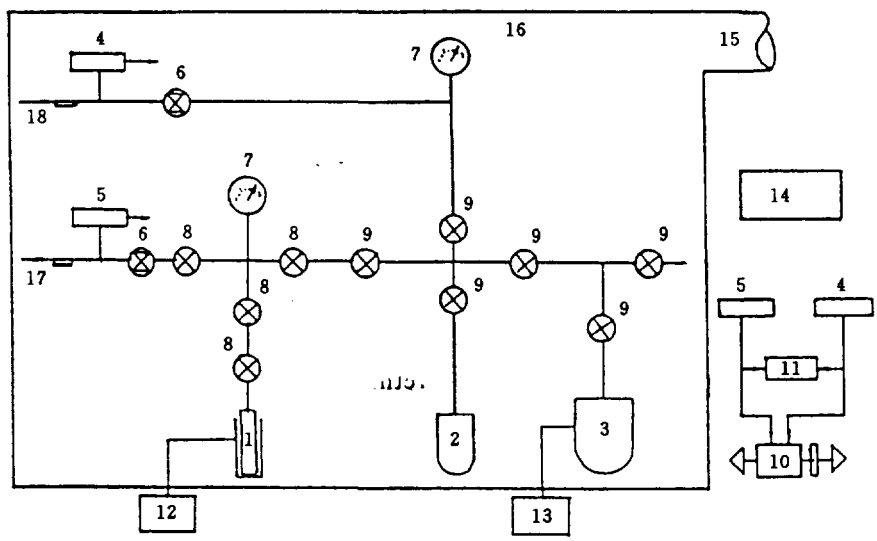

Fig. 2 Handling system diagram of the tritium gas target assembly

1. Tritium gas in pyrophoric uranium; 2. Helium gas bottle; 3. Turbomolecular pumping system;
4. Helium gas pressure transducer; 5. Tritium gas pressure transducer; 6. Metering valves;
7. Pressure gauge; 8. Bellows sealed valves; 9. Valves; 10. Fast–response valve;
11. Alarm; 12. Heater and control unit; 13. Vacuum meter; 14. Tritium gas monitor;
15. Ventilation pipe; 16. Glove box; 17. To Tritium gas cell; 18. To Helium gas cell.

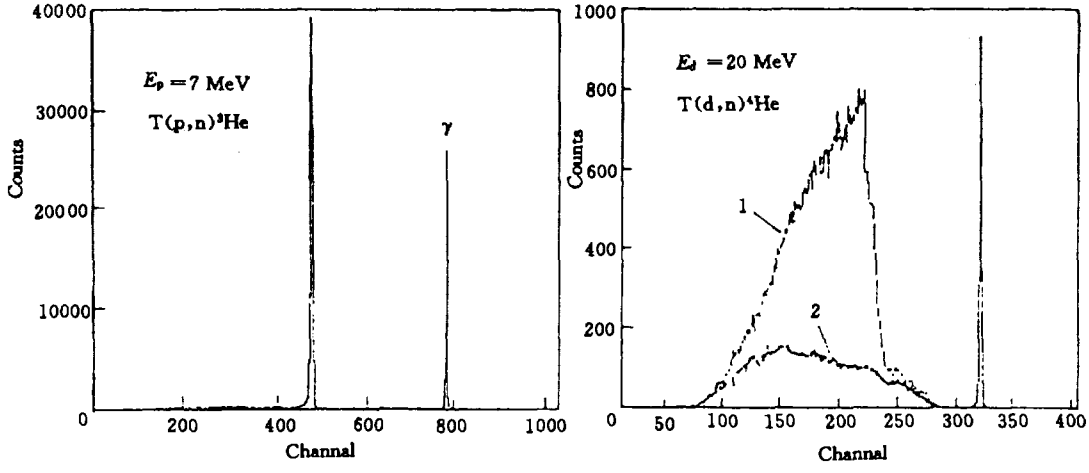

Fig. 3 Neutron TOF spectra of $T(p,n)^3He$ and $T(d,n)^4He$ reaction
$E_p = 7$ MeV and $E_d = 20$ MeV (1 —— Tritium gas in, 2 —— Tritium gas out)

References

[1] J. D. Carlson, Nucl. Inst. and Meth., 113, 541(1973)

[2] C. L. Morris et al., Nucl. Instr. and Meth., 96, 281(1971)

[3] A. B. M. G. Mostafa, Nucl. Instr. and Meth., 125, 493(1975)

[4] Н. И. Фетисов, ПТЭ, 6, 22(1980)

CN9701136

Studies of Fragment Angular Distributions in the Fission of ^{197}Au, ^{207}Pb and ^{209}Bi Induced by Alpha Particles of Energy up to 70 MeV

R. K. Jain J. Rama Rao S. K. Bose

(Department of Physics, VDG Laboratory,
Banaras Hindu University, Varansi–5)

Abstract

The fission fragment angular distributions are measured with Lexan polycarbonate plastics for alpha–particle induced fission of gold, lead and bismuth. The measurements are made at several alpha particle energies between 40 and 70 MeV. At these energies, the relative differential fission cross sections for gold, lead and bismuth acting as targets are measured at several angles between 0° and 180° and the resulted angular distributions are fitted by least square method with Legendre polynomials. The anisotropies $W(0°) / W(90°)$ at several alpha particle energies are measured for the above targets. These data are utilized in the calculation of the energy dependence of K_0^2, the standard deviation of the distribution of the angular momentum projection on the nuclear symmetry axis at the saddle point. The integral cross section for alpha induced fission in each target is determined by numerical integration of the respective differential cross sections measured in the center of mass system. The results are compared with similar data available in the literature which is helpful in resolving some of the discrepancies observed in earlier measurements. Fission cross sections measured for the various reactions are compared with total reaction cross sections calculated with an optical model potential.

Introduction

Fission angular distributions have been studied for years and have been treated as classic examples of transition state theory. Several investigations of fission fragment angular distributions have been reported. Most of these experiments were performed with heavy elements as targets, although a variety of

projectiles was used to induce fission. Angular distributions of fission fragments from targets in the vicinity of lead bombarded with alpha particles have been reported by Coffin and Halpern[1]. The fission fragment angular distributions have been interpreted with the theory suggested by Bohr [2] and developed by Halpern and Strutinski[3] and Griffin[4].

In the present paper, the angular distributions are reported for fragments in the fission of ^{197}Au ^{207}Pb and ^{209}Bi by alpha particles at different energies i. e. 40, 50, 60 and 70 MeV. The fragment anisotropies determined from these distributions are used in calculating the values of K_0^2 for each compound nucleus. The quantity K_0 is defined as the standard deviation of the distribution of the angular momentum projection on the nuclear symmetry axis at the saddle point. The theory[3] postulates that the K distribution of the intrinsic states of a nucleus at the saddle point excitation energy is not altered at the stage of the fission process beyond the saddle point. The evidence[5] exists in support of this postulate. The fission fragment anisotropy is then found to depend on the parameter $p = I_{max}^2 / 4K_0^2$, where K_0^2 is connected with the effective moment of inertia J_{eff} and the nuclear temperature T of the saddle point nucleus by the relation

$$K_0^2 = J_{eff}\ T / h^2 \tag{1}$$

The effective moment of inertia J_{eff} is defined as

$$J_{eff} = J_{\perp} J_{//} / (J_{\perp} - J_{//}) \tag{2}$$

Where $J_{//}$ and $J_{\perp}$ are the moments of inertia about axes parallel to and perpendicular to the fission axis, respectively. On the basis of the Fermi gas model, it is therefore expected that

$$K_0^2 = \frac{J_{eff}(E_x^s)^{1/2}}{h^2 (a_f)^{1/2}} \tag{3}$$

Where E_x^s is the excitation energy and a_f is the nuclear level density parameter, both corresponding to the saddle point configuration of the nucleus. The value of K_0^2, therefore, is extracted from the measurements of the fragment angular distributions.

Liquid drop model calculation[6, 7] indicates a marked change in the deformation of the saddle point for nuclei with X between 0.65 and 0.74,

where $X = (Z^2/A)/(Z^2/A)_{crit}$. Therefore, target nuclei of gold, lead and bismuth were chosen in this investigation. The fission fragments were detected with Lexan plastic detectors. Since essentially all the fission for the above targets is first chance fission, it is simpler to interpret their fission fragment anisotropies than those from heavy elements (uranium region).

1 Experimental Details

1.1 General

The alpha particle beams were obtained from an indigenous variable Energy Cyclotron at Calcutta, India. The collimating system restricts the diameter of the beam at the target to less than 2 mm. The beam current on the target is of the order 50 nA. The total number of alpha particles striking the target was measured with a Faraday cup equipped with a secondary electron suppression device.

The target of fissionable material placed at the centre of a cylindrical tube was bombarded by the collimated beam from the cyclotron. The beam direction is perpendicular to the cylinder axis. The diameter of the cylinder is 9.8 cm and height 5.2 cm[8]. This system is kept in vacuum in a scattering chamber [9]. The fragments emitted from the target embedded themselves in foils (Lexan) arranged at various angles (10°, 20°, ···, 170°). The area over which fission tracks registered in each foil is 1.65 cm × 0.2 cm = 0.33 cm^2, while the Lexan foils are located at a distance of 4.9 cm from the target, consequently the uncertainty in the angular position of the fragments in the detector is less than ± 1.17°. The Lexan foils were etched as described in our earlier paper[10].

1.2 Target Preparation

Targets of gold, lead and bismuth were prepared by evaporating in vacuum the natural elements, in VEC, Calcutta target laboratory. The elements gold and bismuth are monoisotopic. The thickness of each gold and bismuth target is 500 $\mu g/cm^2$ (self support). A ^{207}Pb self supporting target of thickness 500 $\mu g/cm^2$ was made.

1.3 Experimental Observation

The fission fragment track densities were measured for gold, lead and bismuth targets for angles between 10° and 170° in the laboratory system. Da-

ta collected for fissioning nuclei were converted to center–of–mass coordinates assuming (1) full momentum transfer of the incident charged particle to the compound nucleus (2) equal kinetic energy for all fission fragments and (3) symmetric fragment mass distribution. These three conditions are generally more or less satisfied in charged particles induced fission of these nuclei at medium energies as those employed in the present investigation. The kinetic energy release in the center–of–mass system is estimated from the relation [11]

$$E_K = \frac{0.1189\ Z^2}{A^{1/3}} + 7.3\ ,\quad \text{MeV} \tag{4}$$

Where E_K represents the average total kinetic energy of the fission fragments before neutron emission, and Z and A are the atomic and mass numbers of the compound nucleus respectively.

2 Results and Discussion

The analysis of the data essentially consists of the following parts :

(1) Least square fitting of the center–of–mass angular distributions of fission fragments by a series of Legendre polynomials, to draw inferences about the relative orbital angular momentum of the fission fragments.
(2) A comparison of the anisotropy of the angular distribution for different targets as a function of Z^2 / A, to assess the competition between fission and neutron evaporation.
(3) Determination of K_0^2 values from Eq. (5) as given below [12~15]

$$\frac{W(0^\circ)}{W(90^\circ)} = 1 + \frac{I_{max}^2}{8K_0^2} \tag{5}$$

Where $W(0°)$ and $W(90°)$ are the counts of the fragments per unit solid angle at 0° and 90° in the center of mass system, respectively.
(4) Measurement of the total fission cross section by integrating the measured differential cross sections and comparing the results with theory and previous data to resolve discrepancies.

The fission fragment angular distributions were measured in laboratory system for the targets ^{197}Au, ^{207}Pb and ^{209}Bi bombarded with alpha particles. The measured track densities in the laboratory $W_L(\theta)$ are converted into labor-

atory differential cross section ($d\sigma / d\Omega$) using the formula

$$\left(\frac{d\sigma}{d\Omega} \right) = \frac{W_L(\theta)}{\Omega_L \Phi N} \tag{6}$$

Where Ω_L is the laboratory solid angle subtended by the unit area of the detector over which the track density $W_L(\theta)$ is measured, Φ is the incident alpha particle fluence and N is the number of target nuclei per unit area. The laboratory differential cross sections ($d\sigma / d\Omega$) are then converted into center–of–mass differential cross section ($d\sigma / d\Omega$)$_{cm}$, using the relevant transformation equation described in our earlier paper[16].

The relative differential fission cross sections $\frac{d\sigma(\theta^\circ) / d\Omega}{d\sigma(90^\circ) / d\Omega}$ or angular anisotropies $W(\theta^\circ) / W(90^\circ)$ as function of angle θ were deduced from the data of gold, lead and bismuth targets and shown in Fig. 1 for different energies. The dashed, dot–dashed and solid lines in Fig. 1 for gold, lead and bismuth respectively are the best fit to the experimental data obtained using Legendre polynomials with even terms up to $P_6(\cos\theta)$ with coefficients as listed in Table 1. Coefficients higher than A_6 were found to be statistically not significant and hence not included in the table.

In an approximate way, one may expect the average orbital angular momentum of the fission fragments to be given by the l–value of the highest angular momentum term (with statistically significant coefficient) in the Legendre polynomial expansion. On this basis and looking at Table 1, one can conclude that in the presently studied alpha induced fission of gold, lead and bismuth, the orbital angular momentum of the fission fragments generally does not exceed $3\hbar$ while the average incident angular momentum is about $20\hbar$. The difference between the two values is dissipated into the formation of high spin states of the fission fragments as well as into collective rotational degrees of freedom such as rolling friction in some cases.

The experimental anisotropy may be conveniently defined as $W(0^\circ) / W(90^\circ)$ and is listed in Table 1 as a function of the parameter Z^2 / A for the three fissioning nuclei at different energies. It can be seen from Table 1 or Fig. 1 that the anisotropy, $W(0^\circ) / W(90^\circ)$, increases with increasing of incident particle energy. On the one hand, $W(0^\circ) / W(90^\circ)$ decreases with increasing value of Z^2 / A of the target nucleus. This trend is generally observed experimentally but the correlation between anisotropy and Z^2 / A can not be described from a theoretical stand point as fundamental

to the fission process. On the other hand it is most likely to arise from fortuitous effects connected with neutron evaporation before fission. From Table 1 one can notice that for the same bombarding energy of 60 MeV (and consequently for the same angular momentum given to the compound nuclei) the anisotropy in the fission of ($\alpha+^{197}$Au) system is greater than that of ($\alpha+^{207}$Pb) and ($\alpha+^{209}$Bi) system. Qualitatively this can be explained by the comparatively greater probability of the former system for emitting neutrons prior to fission than the latter. This follows from the fact that Z^2/A is proportional to the fissility parameter, and ^{207}Pb and ^{209}Bi having greater fissility than ^{197}Au undergo fission in relative preference to neutron evaporation. Prior neutron emission affects the fission fragment anisotropy in two opposite ways :

(1) Firstly, due to neutron evaporation, the spin distribution of the compound nucleus is smeared out, rather than being sharply aligned, and this effect, in fact, tends to reduce the fission fragment anisotropy.

(2) Secondly, but more importantly, the prior emission of a neutron reduces the available excitation energy for the subsequent fission of the residual fissioning nucleus. There is very clear experimental evidence (Henkel and Brolley)[17] to show that the anisotropy increases very strongly as the excitation energy is lowered by neutron evaporation. It is obvious that the latter effect overweighs the former and causes increased anisotropy.

To check the systematics of the present experiment, we deduced the value of K_0^2 which is the standard deviation of the angular momentum projection on the nuclear symmetry axis in the saddle point configuration which sensitively controls the fission fragment angular distribution. For this purpose we used Eq. (5). Values of I_{max} are estimated from the fusion cross section code FRANPIE[18] which utilizes empirical fusion barriers from Vaz et al.[19] and (for high energy) the critical radius approach of Galin et al.[20]. Values of $W(0°)/W(90°)$, I_{max} and K_0^2 are shown in Table 2 for different incident particle energies. From Table 2 it can be noticed that the value of K_0^2 increases with increasing particle energy and the value of K_0^2 in the fission of ($\alpha+^{209}$Bi) system is greater than that of ($\alpha+^{197}$Au) system or ($\alpha+^{207}$Pb) system. Kapoor et al.[21] also deduced K_0^2 for ^{209}Bi and ^{238}U with different method. They used the angular distribution of the fragments in the center–of–mass system to deduce the values of K_0^2 for various alpha particle bombarding energies on the basis of the model proposed by Halpern and Strutinski[22]. Our present values of K_0^2 are less than the Kapoor's in the case of ^{209}Bi.

The integral cross section for fission at a given energy of the projectile σ_f can be determined by integration over the solid angle, as follows[23].

$$\sigma_f = \frac{2\pi W(90^\circ)}{\Phi N \Omega} \int_0^\pi \frac{W(\theta)}{W(90^\circ)} \sin\theta d\theta$$

Where $W(\theta) / W(90^\circ)$ is the center–of–mass angular distribution for the particular energy of the charged particle involved.

The experimentally measured cross sections are listed in Table 3 for ^{197}Au, ^{207}Pb and ^{209}Bi targets. The errors associated with the (α,f) and cross sections are estimated to be about nearly 5% for the gold, lead and bismuth targets. The measurements of some of these fission cross sections have been made with different methods by different authors. The results of those measurements are listed in Table 3 for comparison with the present data. It can be seen that there are wide discrepancies in the fission cross section measured by different authors with different detectors. In the case of (α+^{197}Au) system Huizenga et al. measured the fission cross section up to only 43 MeV. Our present value 0.45 mb at 40 MeV nearly matches with the value of 0.30 mb of Huizenga et al.[24]. If we interpolate the data of Ralarosy et al.[25], then our present results are found to be less than the fission cross sections measured by Ralarosy et al.[25], but at 50 and 60 MeV our results are more than the fission cross sections measured by Burnett et al.[26]. At 60 MeV our result matches well with the results of Jungerman [27].

In case of (α+^{207}Pb) system, our present value of fission cross section at 40 MeV is found to be greater than the value of Huizenga et al. [24]. If we interpolate the data of Ralarosy et al., then our present results serve to confirm the experimental results of Ralarosy et al.[25] for ^{207}Pb at 50, 60 and 70 MeV, but at 40 MeV our value of fission cross section is found to be greater than the value of Ralarosy et al.[25].

In the case of (α+^{209}Bi) system, our present value of fission cross section at 40 MeV is nearly equal to the value of Huizenga et al. [24], but at 60 MeV our value of fission cross section is found to be greater than the value of Jungerman[27]. If we interpolate the data of Ralarosy et al.[25], then our present results serve to confirm the experimental results of Ralarosy et al.[25] for ^{209}Bi (α,f) at all four energies i. e. 40, 50, 60 and 70 MeV. Our present value of fission cross section is found to be greater than our previous value at 60 MeV[23].

The σ_f / σ_R values as a function of alpha particle energy for gold, lead and bismuth are shown in Table 3. The total reaction cross sections are calculated according to the optical model of Huizenga and Igo[28, 29] using the ALICE computer code[30]. For these targets, σ_f increases quickly with increasing energy. The lower the atomic number of the target, the lower is the contribution of fis-

sion to the reaction cross section.

Acknowledgements

The authors are indebted and thankful to Dr. V. J. Menon for many helpful discussion. The authors are thankful to the entire staff of VECC, Calcutta, India for their effective cooperation. The financial support by the CSIR / UGC, New Delhi is gratefully acknowledged.

Table 1 Anisotropy Z^2 / A & coefficients of Legendre polynomial terms resulting from least square fit of center–of–mass angular distributions from ^{197}Au ^{207}Pb & ^{209}Bi

Target	Energy (Lab) —— MeV	$W(0°)/W(90°)$	Z^2/A	A_0	A_2	A_4	A_6
$^{197}_{79}$Au	40	2.41	32.64	1.2115 ± 0.01870	0.8860 ± 0.0235	0.2390 ± 0.0252	−0.4540 ± 0.02850
	50	2.52	32.64	1.3900 ± 0.0200	0.9730 ± 0.0230	0.2090 ± 0.0250	−0.5340 ± 0.0325
	60	2.58	32.64	1.5200 ± 0.0400	1.0200 ± 0.0240	0.0154 ± 0.0265	0.0527 ± 0.0342
	70	2.62	32.64	1.5400 ± 0.0500	1.0594 ± 0.0244	0.0174 ± 0.0263	0.0447 ± 0.0341
$^{207}_{82}$Pb	40	2.13	33.44	1.2442 ± 0.0320	0.6456 ± 0.0204	0.2448 ± 0.0222	0.0423 ± 0.0293
	50	2.26	33.44	1.3301 ± 0.0330	0.7848 ± 0.0209	0.1726 ± 0.0231	0.0079 ± 0.0288
	60	2.33	33.44	1.3447 ± 0.0340	0.8606 ± 0.0214	0.2616 ± 0.0233	0.0401 ± 0.0303
	70	2.35	33.44	1.4252 ± 0.0412	0.8577 ± 0.0830	0.0550 ± 0.0252	0.0544 ± 0.0312
$^{209}_{83}$Bi	40	2.12	33.92	1.2065 ± 0.0334	0.5812 ± 0.0193	0.2980 ± 0.0215	0.0887 ± 0.0281
	50	2.18	33.92	1.2552 ± 0.0256	0.6483 ± 0.0195	0.2445 ± 0.0216	0.0728 ± 0.0281
	60	2.21	33.92	1.3121 ± 0.0315	0.7417 ± 0.0201	0.1684 ± 0.0219	0.0142 ± 0.0286
	70	2.29	33.92	1.4021 ± 0.0345	0.8626 ± 0.0214	0.0706 ± 0.0229	−0.0085 ± 0.0301

Table 2 Values of I_{max} angular momentum and K_0^2 obtained by Eq. (5) for the various energies of α particles

Target	Energy / MeV	Value of I_{max} / h	$W(0°)$ / $W(90°)$	Value of K_0^2 from Eq. (5)
^{197}Au	40	19	2.41	32.00
	50	23	2.52	43.50
	60	26	2.58	53.48
	70	28	2.62	60.49
^{207}Pb	40	19	2.13	39.93
	50	23	2.26	52.48
	60	26	2.33	63.53
	70	28	2.35	72.59
^{209}Bi	40	19	2.12	40.29
	50	23	2.18	56.04
	60	26	2.21	69.83
	70	28	2.29	75.97

Table 3 Experimental fission and calculated reaction cross section for α particle induced fission of ^{197}Au ^{207}Pb and ^{209}Bi

Target	Energy / MeV	Fission cross section σ_f / mb	Calculated reaction cross section σ_R / mb	σ_f / σ_R	Fission cross section / mb			
					Ref. [24] Huizenga	Ref. [25] Ralarosy	Ref. [26] Burnett	Ref. [27] Jungerman
^{197}Au	40	0.45 ± 0.022	1220.0	0.369×10^{-3}	0.30	0.23	–	–
	50	3.50 ± 0.178	1485.0	2.357×10^{-3}	–	4.50	2.0	–
	60	12.00 ± 0.58	1666.0	7.203×10^{-3}	–	28.00	8.0	10.00
	70	30.00 ± 1.55	1850.0	16.216×10^{-3}	–	45.00	–	–
^{207}Pb	40	1.70 ± 0.080	1680.0	1.012×10^{-3}	0.18	0.28	–	–
	50	20.00 ± 0.90	1805.0	11.080×10^{-3}	–	18.00	–	–
	60	90.00 ± 5.00	1950.0	46.152×10^{-3}	–	95.00	–	–
	70	140.00 ± 7.80	2090.0	66.985×10^{-3}	–	150.00	–	–
^{209}Bi	40	4.20 ± 0.20	1820.0	2.307×10^{-3}	3.0	3.40	–	–
	50	45.00 ± 2.30	2010.0	22.388×10^{-3}	–	60.00	–	–
	60	200.00 ± 9.00	2190.0	91.324×10^{-3}	–	210.0	–	20
	70	250.00 ± 12.0	2340.0	106.837×10^{-3}	–	300.0	–	–

Ref. [24~27] Values interpolated from data given in the Ref.

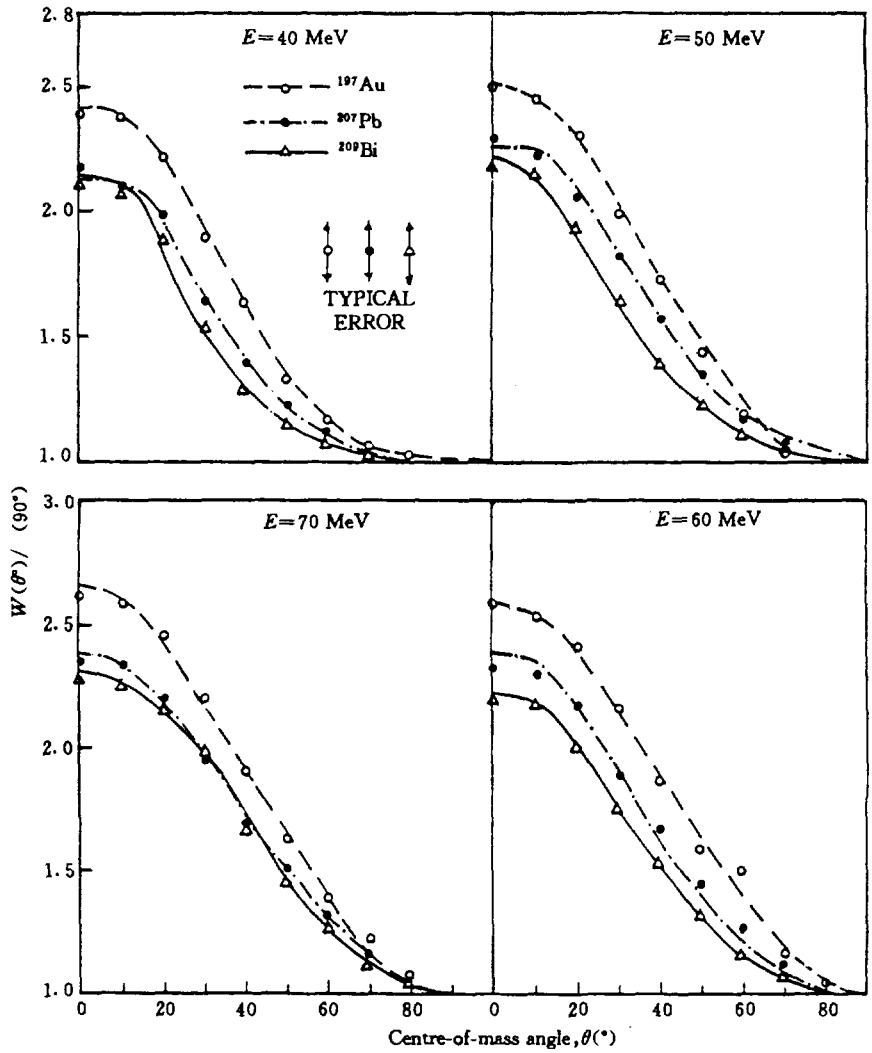

Fig. 1 The anisotropies of fragment angular distributions

References

[1] C. T. Coffin et al., Phys. Rev., 112, 536(1958)

[2] A. Bohr, Proc. Int. Conf. on the Peaceful Use of Atomic Energy, Geneva, Vol. 2, 151(1956)

[3] I. Halpern et al., Proc. Int. Conf. Peaceful Use of Atomic Energy, Geneva, Vol. 15, p. 408(1958)

[4] J. J. Griffin, Phys. Rev., 116, 107(1959)

[5] R. Vandenbosch et al., Phys. Rev., 124, 846(1961)
[6] S. Frankel et al., Phys. Rev., 72, 914(1947)
[7] S. Cohen et al., Ann. Phys. (NY), 22, 406(1963)
[8] R. K. Jain et al., Pramana– J. Phys., 45, 519(1995)
[9] B. B. Baliga et al., Indian, J. Phys., 60A, 465(1986)
[10] A. K. Singh et al., Nucl. Instr. Meth. Phys. Rev., B40 / 41, 1233(1989)
[11] V. E. Viola et al., Phys. Rev., C31, 1550(1985)
[12] Vaz Louis et al., Phys. Rev., 97, 1(1983)
[13] R. H. Iyer et al., DAE Symp. on Nucl. Phys., 33B, 111(1990)
[14] R. K. Jain et al., DAE Symp. on Nucl. Phys., 35B, 290(1992)
[15] Zhang Huanqiao et al., Nucl. Phys., A512, 531(1990)
[16] R. K. Jain et al., Pramana– J. Phys., 39, 85(1992)
[17] R. Henkel et al., Phys. Rev., 103, 1292(1956)
[18] L. C. Vaz, Computer Physics. Communication, 22, 451(1981)
[19] L. C. Vaz et al., Phys. Rep., 69, 373(1981)
[20] J. Galin et al., Phys. Rev., C9, 1018(1974)
[21] S. S. Kapoor et al., Phys. Rev., 149, 965(1966)
[22] I. Halpern et al., Proc. 2nd, UN Int. Conf. on the Peaceful Uses of Atomic Energy, Geneva, 15, 408(1958)
[23] R. K. Jain et al., Indian, J. Phys., 67A, 149(1993)
[24] J. R. Huizenga et al., Phys. Rev., 126, 210(1962)
[25] J. Ralarosy et al., Phys. Rev., 8C, 2372(1973)
[26] D. S. Burnett et al., Phys. Rev., B124, 952(1964)
[27] J. Jungerman, Phys. Rev., 79, 632(1950)
[28] G. Igo, Phys. Rev., 115, 1665(1959)
[29] J. R. Huizenga et al., Nucl. Phys., 29, 462(1962)
[30] M. Blann, Code ALICE / 85 / 300 UCID–20169 (1984)

CN9701137

Cross Section Measurement for Reaction $^{193}Ir(n,2n)^{192m2}Ir$ at 14.7 MeV

Kong Xiangzhong Wang Yongchang Hu Shangbin Yang Jingkang

(Department of Modern Physics, Lanzhou University, Lanzhou)

Abstract

The cross sections induced by neutron on long–lived radionuclides of importance in fusion reactor technology are measured by activation method for $^{193}Ir(n,2n)^{192m2}Ir$ reaction at 14.7 MeV. The neutron fluences are determined by the cross section of $^{93}Nb(n,2n)^{92m}Nb$. The neutron energies in these measurements are determined by cross section ratios for $^{90}Zr(n,2n)^{89}Zr$ and $^{93}Nb(n,2n)^{92m}Nb$ reactions[1].

Introduction

The neutron activation cross sections required for integral calculation in the first wall, blanket and shield of the conceptual design of fusion power reactor have been listed by Cheng[2], reviewed by Cheng[3~5] and Gohar[6]. Working Group I of the 16th International Nuclear Data Committee Meeting identified a set of activation cross sections leading to the production of long–lived radionuclides as a high–priority data request for fusion reactor technology. Long–lived radionuclides are especially important for the assessment of waste disposal, material recycling and maintenance of fusion reactor. Problem still exist for some reactions, for example, for $^{193}Ir(n,2n)^{192m2}Ir$ reaction, the measurement of cross section is still an open question. Therefore we measured the cross section for $^{193}Ir(n,2n)^{192m2}Ir$ by activation method at neutron energy of 14.7 MeV.

1 Experimental Procedure

The decay characteristics of the activation products[7] and natural abundances for the sample under investigation are summarized in Table 1.

Table 1 Reaction and associated decay data of activation products

Reaction	Abundance / %	Half-life / a	E_γ / keV	γ-ray branching
$^{193}Ir(n,2n)^{192m2}Ir$	62.7 ± 0.5	241 ± 9	155.16	0.097 ± 0.004

The irradiation of samples was carried out at the ZF-300-II Intense Neutron Generator at Lanzhou University and lasted 17.25 h with the neutron yield about $(2\sim 6)\times 10^{12}$ n / s. Neutrons were produced by $T(d,n)^4He$ reaction with an effective deuteron beam energy of 125 keV and beam current of 20 mA. The thickness of T-Ti target used in the generator was ≈ 0.9 mg / cm^2. The neutron flux was monitored by an uranium fission chamber so that corrections could be made for variation of neutron yields during the irradiation. The groups of samples were placed at 0° angles relative to the beam direction and centered about the T-Ti target at distances of 2 cm. Cross section for $^{93}Nb(n,2n)^{92m}Nb$ reaction was selected as monitor. The neutron energies at where the samples were determined by the method of cross section ratios for the reactions $^{90}Zr(n,2n)^{89}Zr$ and $^{93}Nb(n,2n)^{92m}Nb$.

After having been irradiated, the gamma ray activities of sample were determined by a CH8403 coaxial high purity germanium detector made in China with a relative efficiency of 20% and an energy resolution of 3 keV at 1.33 MeV. The efficiency of the detector was calibrated using the standard gamma source, Standard Reference Material 4275 was obtained from the National Institute of Standard and Technology. An absolute efficiency calibration curve was obtained at distance of 20 cm from the surface of the germanium crystal. This distance is so far that coincidence losses can be considered to be negligible. In our case, however, we needed to calibrate the efficiency at 2 cm, the actual counting position used because of the weak activity of the sample. Therefore, we selected a set of monoenergetic sources, placed them at two positions (20 and 2 cm) and successively measured their efficiency ratios so that we were able to evaluate the efficiency ratio curve as a function of energy. The absolute efficiency calibration curve at 2 cm was obtained from the calibration curve at 20 cm and the efficiency ratio curve. The error in the absolute efficiency curve at 2 cm was estimated to be $\approx 1.5\%$, while the error of the activity of the standard source is $\approx 1\%$.

More than 4.5 years after the decay of short-lived activities, we started the activity measurements on Ir sample by using a HPGe detector and plastic scintillator-HPGe anti Compton γ-ray spectrometer. The measurement for each sample lasted 9 days.

2 Result

The measured cross section in comparison with evaluated cross section made by Vonach (IRK–89) is summarized in Table 2.

The activation data were processed using conventional experimental technique. The following corrections were made : γ–ray self–absorption in sample, and variation of neutron fluence during irradiation.

The major uncertainties of the measured results were estimated as follow : peak area analysis (8.9%), efficiency of gamma ray (2%), self–absorption gamma ray (5%), standard cross sections (1.5%), decay constant (5.6%), neutron energy determined by the reaction cross section ratio of zirconium and niobium (2%). The total uncertainties is 18.4%. The uncertainties contributed by low energy neutrons from contamination of the neutron source i. e., (d–d) neutrons and scattered neutrons produced in the vicinity of the neutron source and sample package were not considered in this work.

Table 2 Summary of cross section measurement

Reaction	Present work		Vonach (IRK–89)	
	σ / mb	E_n / MeV	σ / mb	E_n / MeV
$^{193}Ir(n,2n)^{192m2}Ir$	154 ± 28	14.7 ± 0.1	184 ± 44	14
			134 ± 80	14.19 ± 0.23[8]

Acknowledgements

We thank the crew of the Intense Neutron Generator at Lanzhou University for performing irradiations and Prof. Lu Hanlin for useful comments and discussions.

References

[1] V. E. Lewis et al., Nucl. Instrum. Method, 174, 141(1980)

[2] E. T. Cheng, Neutron Activation Cross Sections for Fission and Fusion Energy, Argonne, Illinois, September 13～15, 1989

[3] E. T. Cheng, Fusion Technol., 8, 1423(1985)

[4] E. T. Cheng, Proc. Int. Conf. Nuclear Data for Science and Technology, Mito, Japan,

May 30~June 3, (1988)
[5] E. T. Cheng, Nuclear Data Needs for Fusion Energy, Athens. Ohio, Sep. 19~21, 1989
[6] Y. Gohar, Proc. Int. Conf. Nuclear Data for Basic and Applied Science, Santa Fe, New Mexico, May 13~17, p. 15, 1985
[7] E. Browne et al., Table of Radioactive Isotopes, New York, 1986
[8] Lu Hanlin et al., Chin. J. Nucl. Phys., 16(3), 267(1994)

II THEORETICAL CALCULATION

Discrete Level Effect on Spectrum Calculations of Secondary Particles

Zhang Jingshang

(China Nuclear Data Center, CIAE)

Introduction

The adoption of the nuclear model becomes even more important, since the secondary particle energy spectra of each reaction channels are only given by the calculation in the data files. The intercomparison between the large data files has been performed, there are systematical deviations in the secondary neutron emission spectra of (n,2n), (n,nα), etc. and their total neutron emission spectra[1]. A typical example is shown in Fig. 1 for Ni at 14.1 MeV, in which the low energy neutrons (less than several keV) have higher values in ENDF / B–6, then in order JENDL–3, BROND–2, while are missed and have a strong peak at several ten keV, but lower values occur at high energy region in CENDL–2. Based on the calculations with a code, it turns out that the deviations caused by the discrete level effect in the multi–particle emission processes. In Sec. 1 the formulas are given for the analysis, while the conclusion is given in the last section.

1 Formulation of Spectrum Calculations

To keep the parity and angular momentum conservations, the emission rate of the first particle is presented by $W_1^{J\pi,\,J'\pi'}(n,E,\varepsilon_1)$, at n exciton state and excitation energy E with the outgoing energy ε_1, while $J\pi$ and $J'\pi'$ refer to the initial and final J, π states. The total emission rate reads

$$W_T^{J\pi}(n,E) = \sum_b \sum_{J'\pi'} W_b^{J\pi,J'\pi'}(n,E,\varepsilon_1) \tag{1}$$

Defining P function

$$P_1(E,E',n,J',\pi') = \sum_{J\pi} \sigma_a^{J\pi} P^{J\pi}(n) \frac{W_b^{J\pi,J'\pi'}(n,E,\varepsilon_1)}{W_T^{J\pi}(n,E)} \tag{2}$$

where $E' = E - B_1 - \frac{M_c}{M_r}\varepsilon_1$ stands for the residual excitation energy, and M_c, M_r for the masses of compound and residual nuclei. Then the spectrum of the first particle emission is given by

$$\frac{d\sigma}{d\varepsilon_1} = \sum_{J'\pi' n} P_b(E,E',n,J',\pi')$$

The spectrum of the second particle emission can be obtained as follows.

(1) For the continuum emission

The T factor of the second particle emissions for continuum spectrum is given by

$$T_2^{J'\pi'}(E')_c = \frac{1}{2\pi h} \int \sum J''\pi'' \sum_{lj} T_{lj}(\varepsilon)\rho^{J''\pi''}\left(E' - B_2 - \frac{M_r}{M_{r'}}\varepsilon\right) d\varepsilon \tag{3}$$

The angular momentum conservation needs

$$|J' - J''| \leqslant j \leqslant J' + J''; |j - S_2| \leqslant l \leqslant j + S_2$$

where S_2 is the spin of the second particle. The parity conservation needs $(-1)^l = \pi'\pi''$.

(2) For the discrete level emission

The T factor of the second particle emissions for discrete k_{th} lever spectrum is given by

$$T_2^{J'\pi'}(E')_k = \frac{1}{2\pi h} \sum_{lj} T_{lj}(\varepsilon_k) \tag{4}$$

where $\varepsilon_k = \frac{M_{r'}}{M_r}$ ($E' - B_2 - E_k$) is the emission energy of the second particle with the k_{th} level energy E_k, spin I_k and parity π_k.

The angular momentum conservation needs

$$|J' - I_k| < j < J' + I_k; \ |j - S_2| < l < j + S_2$$

The parity conservation needs $(-1)^l = \pi'\pi_k$.

The total emission T factor is

$$T_2^{J'\pi'}(E') = T_2^{J'\pi'}(E')_c + \sum_k T_2^{J'\pi'}(E')_k \tag{5}$$

The total emission rate $T_T^{J'\pi'}$ (E') is given by the summation over all kinds of emitted particles as well as the gamma emission. Thus, the ratio of the second particle emission is obtained by

$$R_2^{J'\pi'}(E') = \frac{T_2^{J'\pi'}(E')}{T_T^{J'\pi'}(E')}$$

Therefore the spectrum of the secondary particle emission is given by

$$\sigma_{1,2}(\varepsilon') = \sum_{J'\pi'} \sum_n P_1(E,E',n,J',\pi') R_2^{J'\pi'}(E') \tag{6}$$

2 Analysis and Conclusion

To indicate the discrete level effect in multi–particle emission processes, the calculations have been performed with UNF code[2, 3]. As the example, the data of neutron spectrum for ^{56}Fe(n,2n) at $E_n = 14$ MeV is shown in Fig. 2. In this case only 11 levels are opened. The real line is the result with the discrete level calculation. But if we only use continuum emission formula instead of the discrete levels the result is given by the dash line. From the results one can see the discrete level effect. Without the discrete levels the spectrum has the characteristic picture given in Fig. 1. The discrete level effect in the spectra calculations gives the strong hard tail and also the low energy part. A extreme example performed by Prof. Liu Tingjin is shown in Fig. 3 for reaction ^{56}Fe(n,nα) at $E_n = 14$ MeV, since only the ground state of the residual nucleus ^{52}Mn is

opened. The discrete level calculations performed in ENDF / B–6, JENDL–3 and BROND–2 have obvious deviation to that of CENDL–2, which only used the continuum level. The calculated result with UNF code is very similar to that of JENDL–3. Based on the analysis above we can draw the conclusion that the discrete level effect must be taken into account in the multi–particle emission processes like TNG, GNASH codes as well as UNF code. Otherwise the neutron spectra would be very unreasonable at some incident energies.

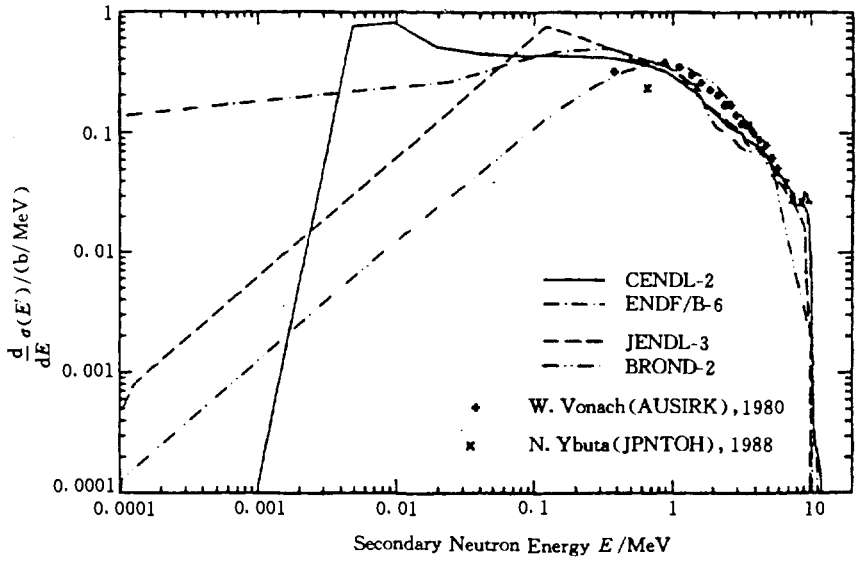

Fig. 1 Ni secondary neutron emission spectrum at 14.1 MeV

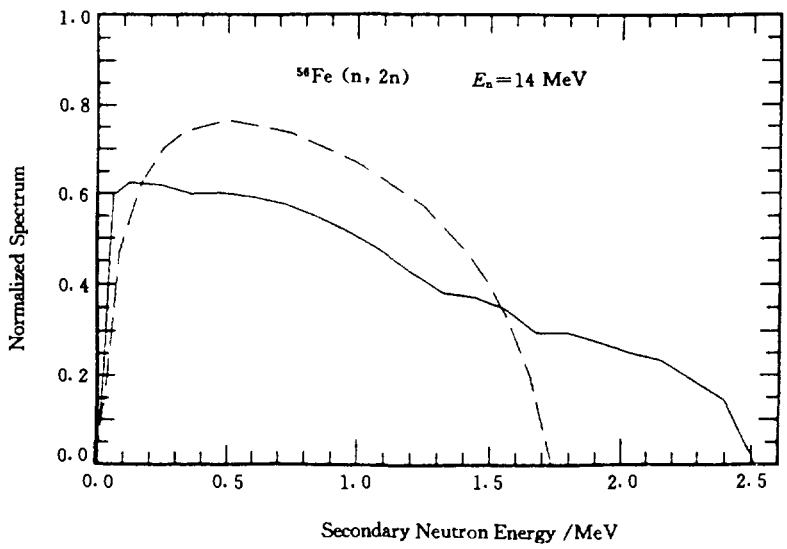

Fig. 2 Neutron spectra of ^{56}Fe(n,2n) at E_n = 14 MeV

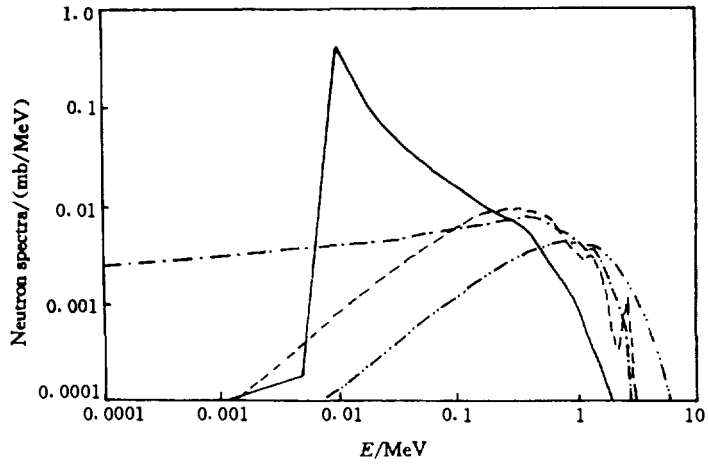

Fig. 3 Neutron spectra of Fe(n,nα) at $E_n = 14$ MeV
(lines are as same as in Fig. 1)

References

[1] Liu Tingjin et al., "Intercomparison of Fe, Cr, Ni Neutron Data from CENDL–2, BROND–2, and ENDF–6, JENDL–3 Liberties", Proc. Conf. on Nuclear Data for Sci Tech., Gatlinberg, USA, 798(1994)

[2] Zhang Jingshang, Nucl. Sci. Eng., 114, 55(1993)

[3] Zhang Jingshang, "Fast Neutron Physics", p. 201, Beijing International Symposium, Sep. 9～13, 1991

CN9701139

n+^{238}U (E_n = 5 MeV) Scattering Angle Distribution Calculation by ECIS95 and Comparison

Wang Shunuan

(China Nuclear Data Center, CIAE)

Abstract

The elastic and inelastic scattering calculations for n+^{238}U (E_n = 5 MeV) within the framework of spherical and deformed nuclear optical model by using ECIS95[1~2] are performed and compared with experimental data and the other coupled channel optical model calculations[3].

ECIS95[1~2] is the latest version of the code ECIS by sequential iteration of coupled channel equation method presented by J. Rayna, which provides an alternative to the conventional matrix method of performing the coupled channel calculations, i. e., which can be used to obtain the knowledge by solving the partial wave Lippmann–Schwinger equation iteratively.

Now, we have met with success in running the code PRECIS on PC486 and ECIS95 on Spart–10 Sun Working Station at CNDC. The ten testing examples with code ECIS95 have been calculated correctly.

In order to make a calculated results comparison between ECIS95 and the other coupled channel optical model calculations described in Ref. [3] in which the rotational deformed nuclei neutron coupled channel calculation code was designed by Yang in 1978 on the computer 6912 made in China[4]. In the calculation and comparison, the n+^{238}U(E_n = 5 MeV) for symmetrical rotational statically deformed coupled channels calculations has been taken as an example.

From the theoretical point of view, the generalization of the spherical spin–orbit potential to a deformed one is not straightforward as others like Coulomb, real and imaginary volume and surface terms of the optical potential would make it appear. In spin 1 / 2 systems it can be obtained from the Dirac equation by eliminating the lower components of the wave function to obtain an equivalent Schrodinger equation for the spherical spin–orbit potential to a deformed one[1]. It then appears in its full Thomas form. In ECIS95 the generalization of the spherical spin–orbit potential to a deformed one has been tak-

ing into account, while in Ref. [3] this generalization is not considered.

In the calculations of Ref. [3] and the present paper, the Ch. Lagrange[5] optical potential parameters have been adopted as shown as the following

real volume term $V=48.5$ MeV

imaginary surface term $W_s=4.7$ MeV

real spin–orbit term $V_{so}=7.5$ MeV

radii and diffusivities r_V, r_s, r_{so} and a_V, a_s, a_{so}

are 1.24, 1.26, 1.24 and 0.62, 0.58, 0.62 fm, respectively.

For β_λ — the static deformation of multipolarity λ, $\lambda=2$ and 4, has been considered with taking $\beta_2=0.216$, $\beta_4=0.06$ in the present ECIS95 calculations, while in the calculations of Ref. [3] only $\lambda=2$ with taking $\beta_2=0.216$ has been considered.

In the calculations of n+^{238}U at $E_n=5$ MeV, the ground state 0^+, the first excitation state 2^+ (0.044 MeV), and the second excitation state 4^+ (0.148 MeV) are dealt with. The calculated results and the experimental data are shown in Fig. 1.

The total elastic scattering on the target ground state of spin 0^+ as a function of angles is shown by — . — . — line for the results of Ref. [3], and ..... line for the present calculations. It can obviously be seen that the peaks especially the deep valleys calculated by ECIS95 are not so strong as the one calculated in Ref. [3]. It seems that the present calculations are much more reasonable due to the effects of the coupling of 2^+ and 4^+ to the ground state of the target have been taking into account. The inelastic scattering to the target state 2^+ as a function of angles are shown by–●–●– line for Ref. [3] calculations and — • — • — line for the present paper. There are some difference at backward angles, but for both cases the forward peaked angular distribution is obvious, even it would be said that the present one more forward peaked from the tendency of the line. The inelastic scattering to the target state spin 4^+ as a function of angle are shown by line with × × × for Ref. [3] and – • – • – line for the present calculations. From Fig. 1 it can be seen clearly that the forward peaked angular distributions are still over there, but the results calculated by ECIS95 is much more powerful than the one presented in Ref. [3].

In Fig. 1, I stands for the experimental data of the elastic scattering angular distribution. As a matter of fact, it is difficult to distinguish the elastic and low energy states inelastic scattering from the experimental point of view. Hence as doing in Ref. [3], putting the scattering of 0^+, 2^+, and 4^+ all together and making a comparison with the elastic scattering experimental data observed have been carried out. The results are shown in Fig.1 by solid line for the calculations of Ref. [3] and the dashed line for the present calculations. From the

comparison it could be point out that there are almost not much more differences in between of the two cases at less than 120 ° angle range, but there are some differences between solid and dashed lines at backangles. General speaking, the experimental data can be well fitted with both calculations.

From the analysis and the comparisons mentioned above, it occurred to us that the ECIS95 code running on Spart–10 Sun working station and PRECIS code running on PC486 work correctly at CNDC. The two codes will certainly be very effectively used on needs of the descriptions of basic nuclear physics problem and nuclear data evaluation calculations as well as many other applications.

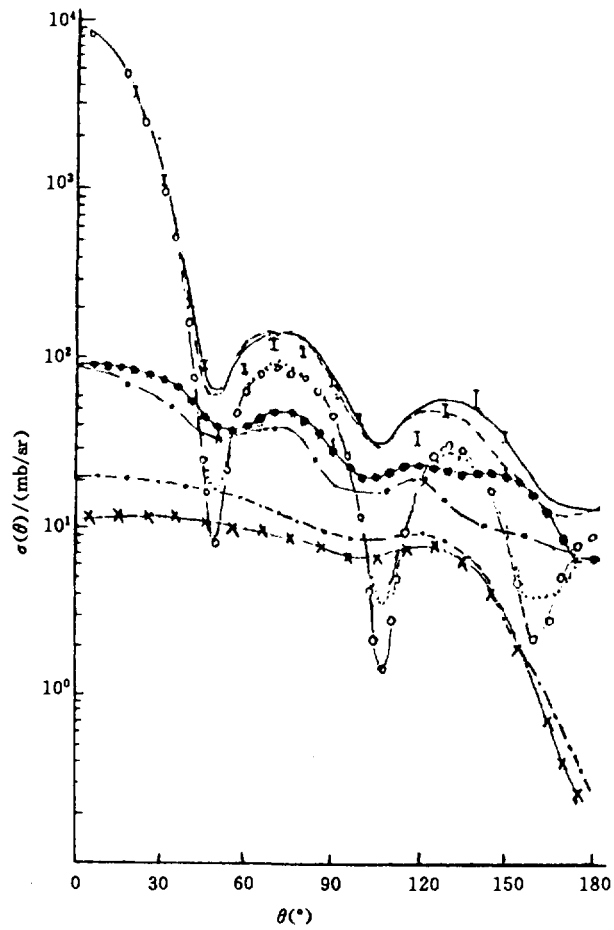

Fig. 1 n+^{238}U (E_n = 5 MeV) scattering angular distribution calculation & comparison

I stands for exp. data; —·—·— Ref. [3], 0^+;

..... present work, 0^+; –●–●– Ref. [3], 2^+, 0, 0447 MeV;

—·—·— present work, 2^+, 0.0447 MeV; × × × Ref. [3], 4^+, 0, 148 MeV;

–·–· present work, 4^+, 0.148 MeV; —— Ref. [3] sum; – – – present work, sum.

Acknowledgments

The author would like very much to thank Prof. J. Raynal who made the code ECIS95, Prof. B. V. Carlson who made the code PRECIS and presented the nice lectures on the Workshop and also helped with making all of the codes copies at ICTP, and Prof. E. Sartori who sent the Note CEA–N–2772 (Notes on ECIS94).

The author also acknowledges IAEA, UNESCO, ICTP and ENEA for the support of attending the Workshop.

References

[1] J. Raynal, Notes on ECIS94–Note CEN–N–2772(1994)

[2] B. V. Carlson, H4. SMR / 921–3, Workshop on Nuclear Reaction Data and Nuclear Reactors–Phys., Design and Safety, 15 Apr.~ 17 May, 1996, Miramare Trieste, Italy

[3] Shen Qingbiao et al., hsj–78228 (lljs) of CNDC, CIAE, 1980

[4] Yang Zesen et al., 6912 Computer Neutron Rotation Nuclei Coupled Channel Calculations Code, Department of Physics, Peking University, 1978

[5] Ch. Lagrange, JAERI–M–5984, p. 58 (1975)

CN9701140

Calculation of Various Cross Sections for $n+^{169}Tm$ Reaction in Energy Range up to 100 MeV

Shen Qingbiao Yu Baosheng Cai Dunjiu

(China Nuclear Data Center, CIAE)

Abstract

The calculated results show that the activation products $^{168, 167, 166, 165}Tm$ are important neutron monitor reaction products for $n+^{169}Tm$ reaction in energy range up to 100 MeV.

Introduction

The activation products ^{168}Tm (half life is 93.1 d), ^{167}Tm (9.25 d), ^{166}Tm (7.7 h), and ^{165}Tm (30.06 h) can be produced from n+^{169}Tm reaction through (n,2n), (n,3n), (n,4n), and (n,5n) reactions, respectively.

In order to determine the neutron optical potential parameters for n+^{169}Tm reaction in the energy region up to 100 MeV, more neutron experimental data of ^{169}Tm, some nonelastic scattering cross sections of W and Pb, and some total cross sections of neighboring nucleus ^{165}Ho above 20 MeV were used. Then various cross sections of n+^{169}Tm reaction were calculated.

1 Theories and Parameters

The calculation was made with the program SPEC[1] including the first to the sixth particle emission processes, in which the optical model, evaporation model, the master equation of exciton model[2], and the preequilibrium and direct reaction mechanisms of γ emission[3] are included. The direct inelastic scattering cross sections were obtained by the collective excitation distorted–wave Born approximation[4]. The compound–nucleus elastic scattering contributions were calculated by Hauser–Feshbach model.

For composite particle emissions, the pick–up mechanism of cluster formation[5~7] was included in the first and second particle emission processes.

Based on various neutron experimental data of ^{169}Tm and neighboring nucleus W, Pb, and ^{165}Ho from EXFOR library, a set of optimum neutron optical potential parameters in the energy region 2~ 100 MeV was obtained as follows:

$$V = 56.2617 - 0.32366E + 0.0006542E^2 - 24.0(N - Z)/A, \quad (1)$$

$$W_s = \max\{\ 0,\ 7.66205 - 0.037223E - 12.0(\ N - Z\ )/A\ \}, \quad (2)$$

$$W_v = \max\{\ 0,\ -1.42450 + 0.20087E - 0.0011638E^2\ \}, \quad (3)$$

$$U_{so} = 6.2, \quad (4)$$

$$r_r = 1.11857,\ r_s = 1.37404,\ r_v = 1.38091,\ r_{so} = 1.11857, \quad (5)$$

$$a_r = 0.77746,\ a_s = 0.53649,\ a_v = 0.32000,\ a_{so} = 0.77746, \quad (6)$$

The Gilbert–Cameron level density formula[8] is applied in our calculations, and the exciton model constant K is taken as 1500 MeV^3.

2 Calculated Results and Analyses

Fig. 1 shows the comparison of neutron total cross sections between the calculated values and the experimental data in the energy region 2~ 100 MeV for n+^{169}Tm reaction. The theoretical values are in good agreement with the experimental data. Fig. 2 gives the comparison of calculated and experimental (n,2n) cross sections of ^{169}Tm. Fig. 3 shows the comparison of (n,3n) and (n,4n) cross sections between the calculated values and the experimental data for n+^{169}Tm reaction.They basically agree with the experimental data.

The experimental data and calculated results show that the larger values of (n,2n) cross sections producing ^{168}Tm are lying in 10~ 20 MeV energy region; for (n,3n) reaction producing ^{167}Tm in 18~ 32 MeV; for (n,4n) reaction producing ^{166}Tm in 24~ 44 MeV; and for (n,5n) reaction producing ^{165}Tm in 38~ 54 MeV.

3 Summary

Based on the available experimental data, a set of neutron optical potential parameters for ^{169}Tm in energies of 2~ 100 MeV was obtained. Then many nuclear data for n+^{169}Tm reaction were calculated based on optical model, evaporation model and exciton model. Because the calculated results for many reactions are in pretty agreement with the available experimental data, the predicted production cross sections for ^{169}Tm(n,x)$^{168,\ 167,\ 166,\ 165}$Tm reactions are reasonable.

The calculated results show that ^{169}Tm(n,x)$^{168,\ 167,\ 166,\ 165}$Tm reactions are important neutron monitor reactions in the energy range up to 100 MeV.

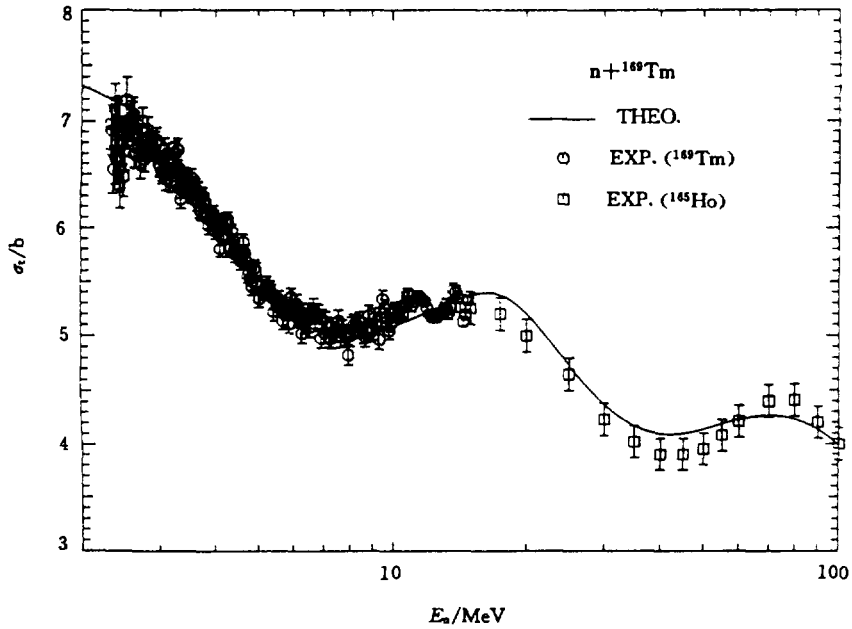

Fig. 1 Comparison of neutron total cross sections of ^{169}Tm

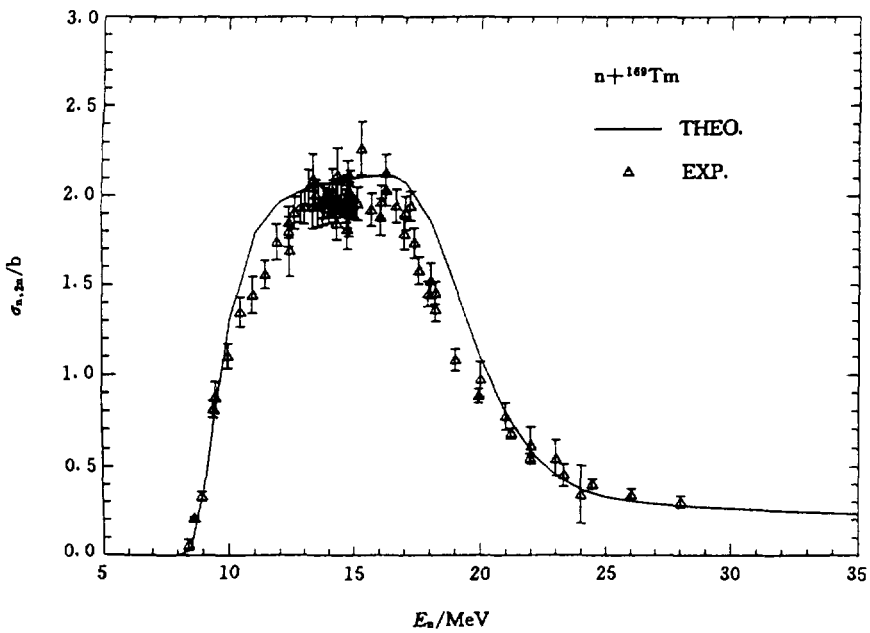

Fig. 2 Comparison of (n,2n) cross sections of ^{169}Tm

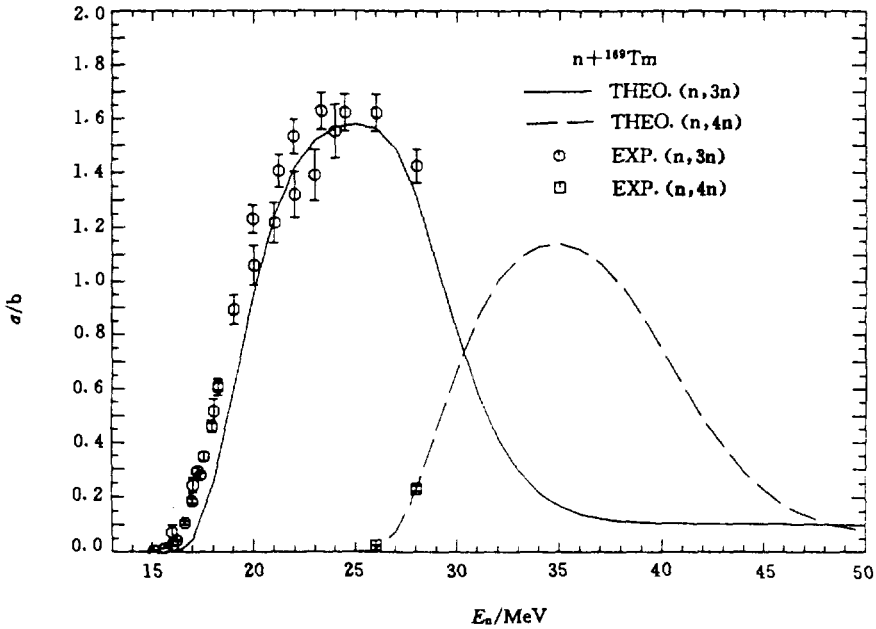

Fig. 3 Comparison of (n,3n) and (n,4n) cross sections of ^{169}Tm

References

[1] Shen Qingbiao et al., CNDP, 11, 28(1994)

[2] M. Blann, Ann. Rev. Nucl. Sci., 25, 123(1975)

[3] J. M. Akkermans et al., Phys. Let., B157, 95(1985)

[4] P. D. Kunz, Distorted Wave Code DWUCK4. University of Colorado, unpublished

[5] A. Iwamoto et al., Phys. Rev., C26, 1821(1982)

[6] K. Sato et al., Phys. Rev. C28, 1527(1983)

[7] Zhang Jingshang et al., Commun. in Theor. Phys., (Beijing, China) 10, 33(1988)

[8] A. Gilbert, C. G. W. Cameron, Can. J. Phys., 43, 1446(1965)

CN9701141

Excitation Functions of Proton Induced Reactions on ^{52}Cr in the Energy up to 30 MeV

Xu Xiaoping Han Yinlu Zhuang Youxiang

(China Nuclear Data Center, CIAE)

Abstract

A set of proton optical potential parameters is obtained on chromium from threshold to 65.0 MeV based on the available experimental data, and the excitation functions were evaluated and calculated for $^{52}Cr(p,n)$, (p,p'), (p,α), $(p,^{3}He)$, (p,d), (p,t), (p,2n), (p,np+pn), $(p,n\alpha+\alpha n)$, (p,2p) and (p,3n) from respective threshold to 30.0 MeV.

Introduction

Studies of excitation functions of charged particles induced reactions are of considerable significance for nuclear science and technology. Compared with neutron experimental data, the charged particles data are scarce, it is necessary to collect and calculate the cross sections according to some theoretical models. The purpose of this paper is to report the set of evaluated and calculated results of $p+^{52}Cr$ reaction in the proton energy up to 30.0 MeV.

1 Evaluation of Experimental Data

The angular distributions of proton elastic scattering on chromium have been reported at 7.75 MeV, 9.76 MeV, 10.0 MeV, 12.0 MeV, 14.1 MeV and 14.3 MeV [1, 2]. There are a few reaction cross sections for p+Cr measured by some laboratories [3,4]. Because the isotope abundances of natural chromium are ^{52}Cr : 83.97%, ^{53}Cr : 9.50%, ^{50}Cr : 4.35%, ^{54}Cr : 2.36%, most of the Cr samples are not in a single isotope of chromium.

Excitation functions of $^{52}Cr(p,n)^{52m,g}Mn$[1, 5~19], $^{52}Cr(p,2n)^{51}Mn$[7, 9, 10, 16, 19], $^{52}Cr(p,np+pn)^{51}Cr$[1, 7, 9], $^{52}Cr(p,n\alpha+\alpha n)^{48}V$[19] have been reported at low bombarding energies and studied by the optical model. The errors lie between 6% and 15%. The measured data are available from threshold energy to 29.5

MeV. The corrections for the experimental data have been made on the basis of the new branching ratio[20]. The corrected results are shown in Table 1.

Table 1 Comparison of the corrected data to the original data for $^{52}Cr(p,n)^{52}Mn$ cross sections

J. Wing (1962)				
E_p / MeV	σ of ^{52g}Mn / mb		σ of ^{52m}Mn / mb	
	old	new	old	new
5.8	4.2	4.23	0.2	0.25
5.8	7.7	7.76	0.4	0.5
5.9	20.0	20.2	1.3	1.6
6.0	28.0	28.2	1.1	1.4
6.4	158.0	159.2	11.0	13.8
7.0	210.0	211.6	23.0	28.8
7.1	220.0	221.6	23.0	28.0
7.4	224.0	225.7	31.0	38.8
8.0	250.0	251.9	44.0	55.0
8.1	260.0	262.0	41.0	51.3
8.4	281.0	283.0	51.0	63.8
8.9	296.0	298.3	60.0	75.0
9.0	288.0	290.2	65.0	81.3
9.1	344.0	346.2	84.0	105.0
9.2	350.0	352.7	69.0	86.3
9.9	326.0	328.4	79.0	98.8
10.1	365.0	367.8	88.0	110.0
10.5	370.0	372.8	98.0	122.5
Linder (1959)				
E_p / MeV	σ of ^{52g}Mn / mb		σ of ^{52m}Mn / mb	
	old	new	old	new
6.0	2.0	1.83		
7.5	128.0	117.0	21.2	19.0
10.0	327.2	358.0	116.0	106.0
10.1	312.0	285.0	104.0	95.0
12.5	410.0	374.7	203.0	185.0
16.0	265.0	242.0	197.0	180.0

Note : The β branching ratios of the old data are 99.0% for ^{52m}Mn, 25.0% for ^{52g}Mn; the β branching ratios published in 1978 by C. M. Lederer and Virginia S. Shirley[20] are 98.25% for ^{52m}Mn, 28.0% for ^{52g}Mn.

Most of these data were measured using the stacked–foil technique. In recent years, in order to check the incident proton energy, the energy degradation in the stack, and the beam intensity, appropriate monitor foils were inserted in each stack. The foils used were made of Cu and Ni for the proton beam and were cut from high purity materials of different thickness. The chemical separation, coincidence technique, Ge–Li detector were used in these experiments.

The experimental data for ^{52}Cr(p,2n) and (p,np) reactions cross sections measured by V. N. Levkovskij (1991)[19] are used to check the calculated results.

2 Theories and Parameters

The optimum proton optical potential parameters of Cr were searched automatically by APCOM[21] to fit the experimental data of reaction cross sections and differential cross sections simultaneously for p+^{52}Cr with incident proton energies of 2.0~65.0 MeV, which are based on the optical model, evaporation model, exciton model of preequilibrium emission theory, the multi–particle and hole state densities considered the Pauli exclusion principle in the exciton model. Because the experimental data of p+^{52}Cr are less, the experimental data of p+^{Nat}Cr reaction cross section were used in our calculation, the set of best proton optical potential parameters on ^{52}Cr was obtained as follows :

$$V = 45.6623 - 0.3075E - 0.00080727E^2 + \frac{24.0(N-Z)}{A} + \frac{0.4Z}{A^{1/3}}$$

Surface absorbed potential,

$$W_s = \max\{0.0,\ 10.11569 - 0.15985E + 12.0(N-Z)/A\}$$

Volume absorbed potential,

$$W_v = \max\{0.0,\ -0.176536 + 0.079064E - 0.00069421E^2\}$$

$$U_{so} = 6.2,$$

$$r_c = 1.85,\quad r_{so} = r_r = 1.27913,\quad r_s = 1.15420,\quad r_v = 1.75990,$$

$$a_{so} = a_r = 0.55839,\quad a_s = 0.43289,\quad a_v = 0.66545.$$

Using this set of proton optical potential parameters on chromium, all reaction cross sections were calculated by code CUNF[22]. The pair corrections, the level densities and the discrete levels with their spins and parities are obtained from Ref. [23] in our calculation. Some other charged particle and neutron optical potential parameters, the level density parameter of each chan-

nel and the free parameter of square of the average two–body interaction matrix element K in preequilibrium exciton model were adjusted. The exciton model parameter K was taken as 600 MeV^3.

The direct inelastic cross sections were calculated by DWUCK–4 [24] and the proton performance factor was taken as 0.25.

3 Results and Discussion

The differential cross sections for p + ^{Nat}Cr are shown in Fig. 1, we have observed that the theoretical calculations are in good agreement with the measured data at the proton energy from 7.75 MeV to 14.3 MeV. Fig. 2 shows the comparison of total proton reaction cross sections on chromium in the energy region 2.0 ~ 65.0 MeV between the theoretical values (solid line) and the experimental data. The calculated results (solid line) are in good agreement with the experimental data and systematics results (the first two points) by B. Buck[25].

The cross sections for $^{52}Cr(p,n)^{52}Mn$ reaction are shown in Fig. 3. The experimental data are the $^{52}Cr(p,n_0)^{52}Mn$ and $^{52}Cr(p,n)^{52}Mn^m$ reaction cross sections, respectively. The theoretical results (solid line) are reasonably larger than the experimental values.

Because some different channels have the same residual nuclei, such as (p,np), (p,pn) and (p,d); (p,nα), (p,αn) and (p,2dn) et al.; (p,^{3}He) and (p,2pn); (p,α), (p,2d), (p,pnd), (p,2n2p) et al., the cross sections obtained by measuring the residual nuclei are the sum of all the corresponding reaction channels. There are some differences between the experimental data and the calculated results, but most of them are in the error permitted range of each channel.

Fig. 4 shows the comparison of the cross sections of $^{52}Cr(p,2n)^{51}Mn$, $^{52}Cr(p,np+pn)^{51}Cr$ and $^{52}Cr(p,np+pn+d+2n)$ reaction between the theoretical results and the experimental data[19]. There are excellent agreement between theoretical and experimental cross sections [4, 7] for $^{52}Cr(p,2n)^{52}Mn$ reaction. The calculated cross sections for $^{52}Cr(p,np+pn)^{51}Cr$ are larger than the experimental data[4,7]. Compared the calculated cross sections for (p,np+pn+d+2n) with the experimental data[19], the experimental data are larger than that of the theoretical results. The cross section of $^{52}Cr(p,n\alpha+\alpha n)^{48}V$ reaction is given in Fig. 5, the theoretical results basically agree with the experimental data [19]; the measuring error is large for $E_p < 26$ MeV probably, because the cross sections are too small.

Fig. 6 illustrates (p,p′), (p,α), (p,^{3}He), (p,d), (p,t), (p,2p), (p,3n) reaction cross sections which have no experimental data. The curves′ trend is reasonable according to the respective channel of some other nuclei which have experimen-

tal data.

4 Conclusions

Based on the available experimental data of chromium, a set of proton optical potential parameters at 2.0~65.0 MeV is obtained. With adjusting the level density of each channel, the calculated nuclear data are in reasonable agreement with the experimental data and might predict some characters of some reaction channels which have no experimental data up to now.

Acknowledgements

One of the authors (Xu) thanks to Drs. Zhang Jingshang, Shen Qingbiao and Su Zongdi for their very kind help and suggestions. This work is supported by CNDC.

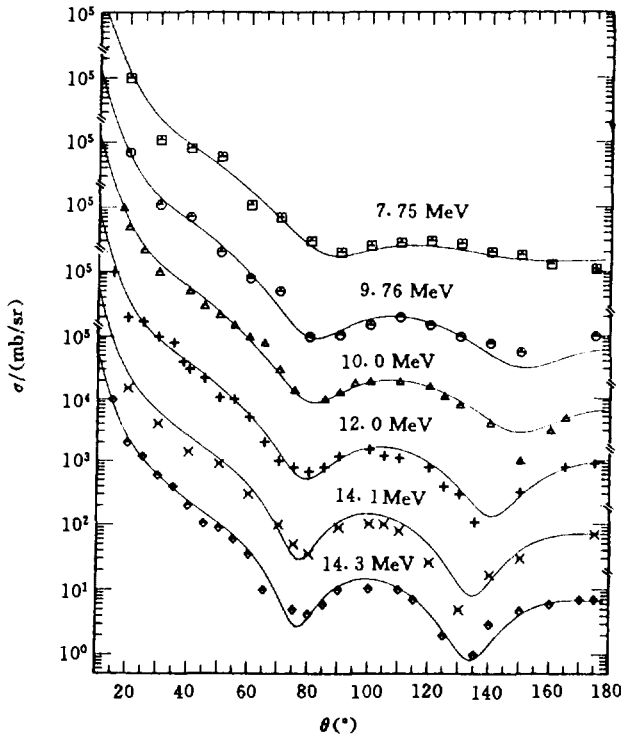

Fig. 1 $^{52}Cr(p,p)^{52}Cr$ differential cross section

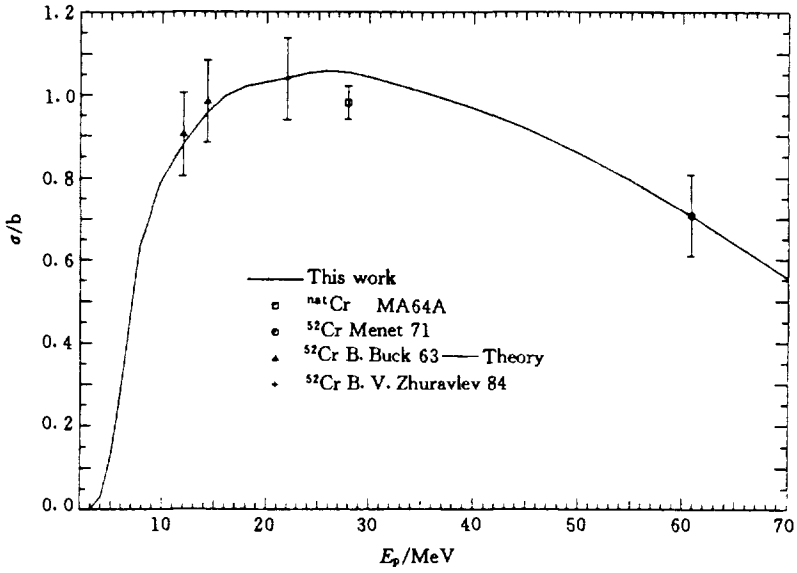

Fig. 2 Cr total proton reaction cross section

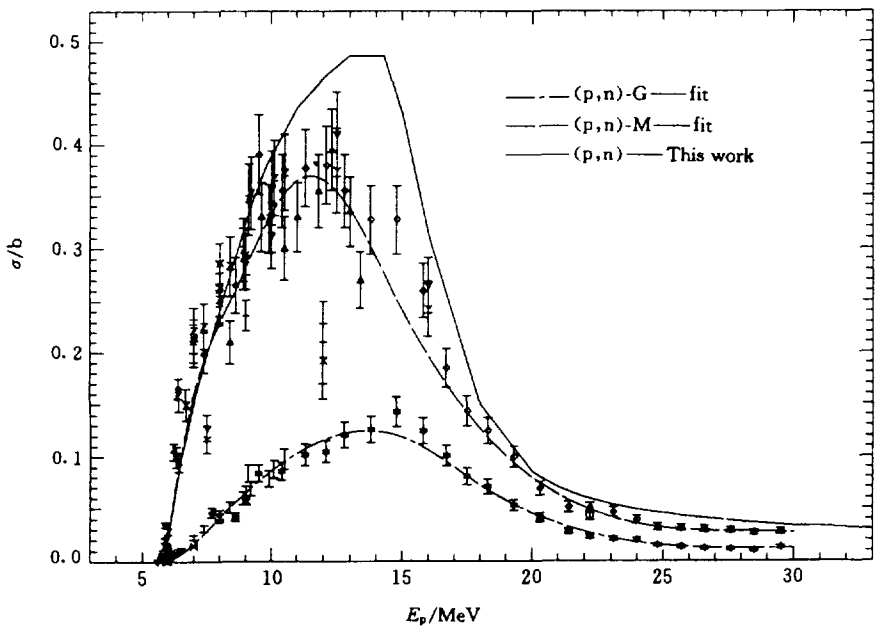

Fig. 3 $^{52}Cr(p,n)^{52}Mn$ cross section

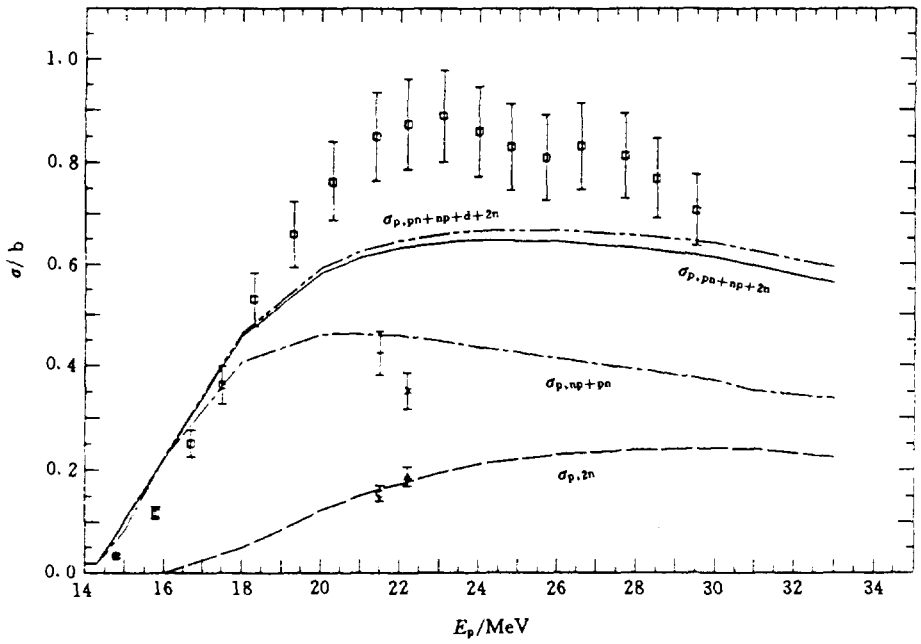

Fig. 4 $^{52}Cr(p,2n)^{51}Mn$, $^{52}Cr(p,np+pn)^{51}Cr$ & $^{52}Cr(p,np+pn+d+2n)$ cross sections

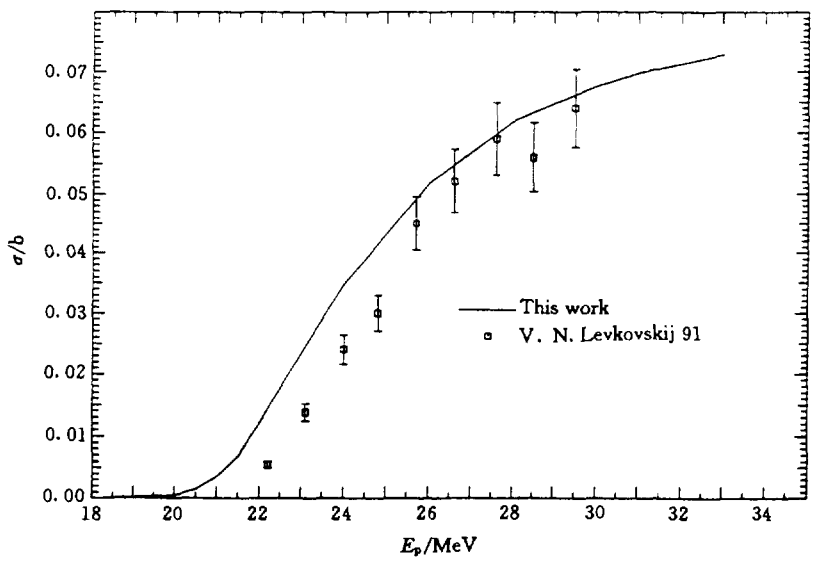

Fig. 5 $^{52}Cr(p,n\alpha+\alpha n)^{48}V$ cross sections

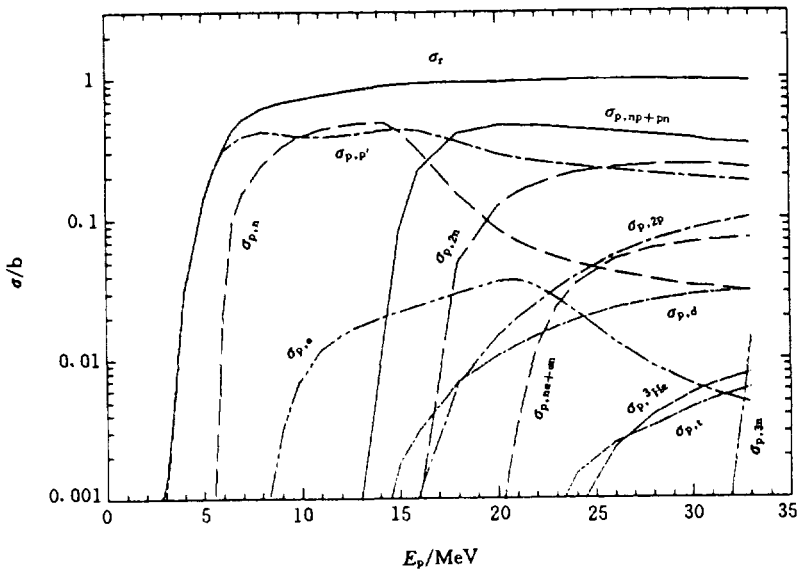

Fig. 6 The reaction cross sections of p+^{52}Cr

References

[1] C. Hu et al., Phys. Soc., Japan, 14, 861(1959)

[2] K. Kikuchi et al., Phys. Soc., Japan, 14, 121(1959)

[3] W. Bauhoff, Atomic Data and Nuclear Data Tables, 35, No. 3(1986)

[4] B. V. Zhuravlev et al., Sov. Nucl. Phys., 39, 264(1984)

[5] A. E. Awtropov et al., 31th Annual Conf. on Nucl. Spect. and Nucl. Stru., Lengrd, 316(1980)

[6] A. V. Muminov et al., Atom. Energy, 49(2), 101(1980)

[7] B. L. Cohen et al., Phys. Rev., 99, 718(1955)

[8] B. Linder et al., Phys. Rev., 114, 322(1955)

[9] D. J. Reuland et al., Inorg. Nucl. Chem., 31, 1915(1961)

[10] E. A. Skakum et al., 36th All Unoin Conf. on Nucl. Spec. and Nucl. Stru., Kharkov, 277(1986)

[11] F. Beohm et al., Helv. Phys. Acta, 25, 599(1952)

[12] H. G. Blosser et al., Phys. Rev., 100, 1340(1955)

[13] H. Takatani et al., Phys. Rev., 125, 291(1962)

[14] J. Wing et al., Phys. Rev., 128, 280(1962)

[15] L. P. Remsberg et al., Phys. Rev., 130, 2069(1963)
[16] L. Valintani et al., Nucl. Phys., 62, 81(1965)
[17] S. Tanaka et al., Phys. Soc. of Japan, 59, 14, 1296(1959)
[18] V. N. Levkovskij, 35th All Union Conf. on Nucl. Spec. and Nucl. Stru., Leningrad, 369(1985)
[19] V. N. Levkovskij, B LEVKOVSKIJ (1991)
[20] C. M. Lederer, Tables of Isotope (1978)
[21] Shen Qingbiao, Commu. Nucl. Data Progress, 7, 41(1992)
[22] Zhang Jingshang, Commu. Nucl. Data Progress, 7, 14(1992)
[23] Su Zongdi et al., Commu. Nucl. Data Progress, 12, 83(1994)
[24] P. D. Kunz, Distorted Wave Code Dwuck4. University of Colorado
[25] B. Buck, Phys. Rev., 130, N2, 712(1963)
[26] Ma Gonggui et al., Commu. Nucl. Data Progress, 6, 94(1991)
[27] R. P. Ward et al., Atomic Data and Nuclear Data Tables, V48, 329(1991)
[28] A. Bredbacha et al., Nucl. Phys., A574, 397(1994)
[29] T. Yamagata et al., Nucl. Phys., A589, 425(1995)
[30] C. Kalbach et al., Z. Phys., A283, 401(1977)

CN9701142

Calculation of Neutron Induced Reaction on ^{103}Rh in Energy from 0.002 to 25 MeV

Sun Xiuquan Zhang Zhengjun
(Department of Physics, Northwest University, Shaanxi)

Han Yinlu Shen Qingbiao
(China Nuclear Data Center, CIAE)

Abstract

A set of neutron optical potential parameters for the energy from 0.002 to 25 MeV is obtained on the basis of available experimental data. Based on this set of optical potential parameters, the elastic scattering angular distributions and all cross sections of neutron induced reaction on ^{103}Rh are calculated. The calculated results reproduce the experimental data well.

Introduction

The cross sections of neutron induced reaction on ^{103}Rh are important for nuclear science and technology. Because there are more experimental data of total cross sections and elastic angular distributions of ^{103}Rh, a set of neutron optical potential parameters can be obtained, with which the cross section of reaction channel with less experimental data can be calculated and it is referential to calculation of the neighbor nuclei which experimental data are less. The purpose of this paper is to present the optical potential parameters and give out the calculated data of all cross sections and elastic scattering angular distributions of ^{103}Rh in induced energy from 0.002 to 25 MeV.

1 Theoretical Model and The Parameters

The code APOM94[1], DWUCK4[2] and SUNF[3] are used in our calculations. The experimental data are taken from EXFOR library. The nuclear discrete levels are taken from Ref. [4]. The parameters of nuclear levels densities and giant dipole resonance are taken from Ref. [5].

The code APOM94 is a program by which the best neutron optical potential parameters can be adjusted automatically to fit the relevant experimental data for total cross sections, nonelastic scattering cross sections and elastic scattering angular distributions. A set of optimum neutron optical potential parameters of ^{103}Rh are obtained as follows :

$$V = 55.26119 - 0.40604E + 0.0015407E^2 - 24.0\ (N - Z)/A,$$
$$W_S = \max\{0.0,\ 9.17634 + 0.22248E - 12.0\ (N - Z)/A\},$$
$$W_V = \max\{0.0,\ -1.56148 + 0.21883E - 0.074714E^2\},$$
$$U_{SO} = 6.2,$$
$$r_R = 1.17754,\quad r_S = 1.38190,\quad r_V = 1.26103\quad r_{SO} = 1.17754,$$
$$a_R = 0.74980,\quad a_S = 0.41142,\quad a_V = 0.58002\quad a_{SO} = 0.74980,$$

The direct inelastic scattering cross sections are calculated by code DWUCK4 on the basis of this set of neutron optical potential parameters. Through adjusting the optical potential parameters of proton, alpha, ^{3}He, deuteron and triton particles, level densities and giant dipole resonance parameters, all reaction cross sections are calculated by using the code SUNF.

The exciton model parameter K is taken as 400 MeV^3.

2 Calculation Results and Analyses

Fig. 1 shows the comparison of neutron total cross section between the calculated results and experimental data in the energy region from 0.01 to 25 MeV. The theoretical values reproduce the experimental data very well. The comparison between calculated values and experimental data of the elastic scattering angular distributions are shown in Figs. 2a, 2b and 2c. The theoretical values are in good agreement with the experimental data. From Fig. 3 we can see that the theoretical values of elastic scattering cross sections are roughly in agreement with the experimental data. Because of the elastic scattering angular distributions experimental data are more and the theoretical values reproduce the experimental data very well, we can draw a conclusion that the experimental data of the elastic cross sections are not well enough. Fig. 4 shows that theoretical values of (n,γ) cross sections are in good agreement with experimental data in energy from 0.002 to 1.0 MeV and the energy points $E_n = 14.6$ MeV and $E_n = 14.06$ MeV[6, 7]. But calculated data are lower in the energy region from 1.0 to 4.0 MeV than experimental data which given by Ref. [8]. Theoretical values and experimental data of (n,2n) cross section of ^{103}Rh are shown in Fig. 5. Our calculated results are in agreement basically with the experimental data which reported by Refs. [9, 10] and obviously higher than which reported by Refs. [11, 12]. The tendency of our calculated results is more reasonable. Fig. 6 indicates theoretical values (n,3n) reaction cross section are in good agreement with the experimental data. Various calculated cross sections are shown in Fig. 7. The (n,p) and (n,t) reaction cross section curves pass through the existent experimental error bars[13, 14], respectively, while the (n,α) reaction cross section curve only pass through the experimental data in Ref. [15].

3 Conclusions

Based on the experimental data of ^{103}Rh and using the code APOM94, we get a set of optimum neutron optical potential parameters for ^{103}Rh in the energy region from 0.002 to 25 MeV. Using the code DWUCK4 and SUNF and through adjusting proton, alpha, deuteron, triton charged particle optical potential parameters, level densities and giant dipole resonance parameters the various cross section of neutron induced reaction are obtained. The calculated results reproduce the experimental data well.

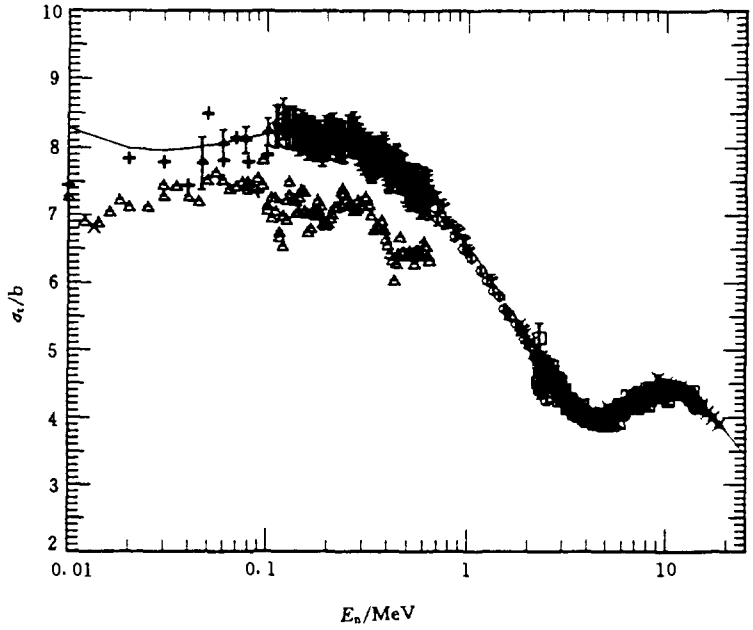

Fig. 1 The total cross section

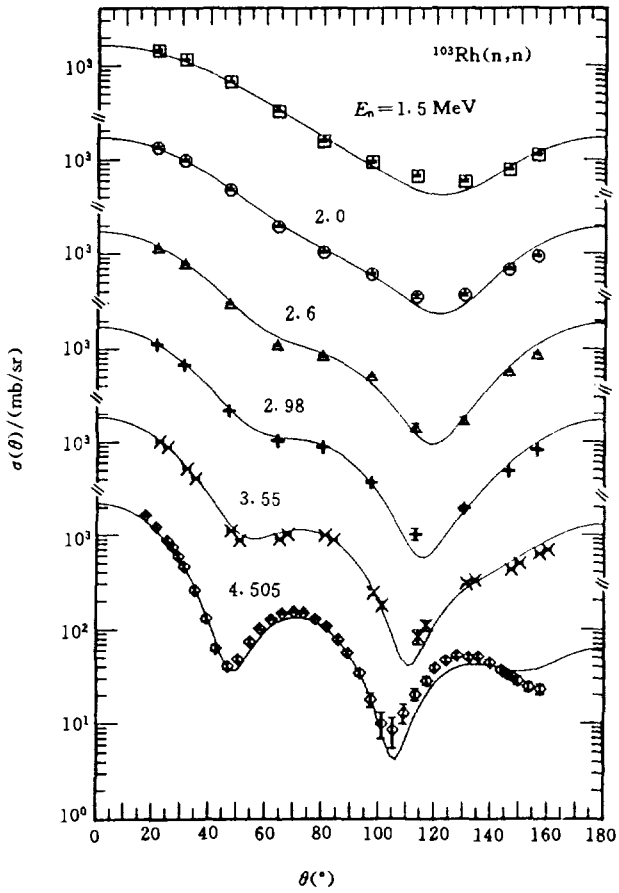

Fig. 2a The elastic scattering angular distribution

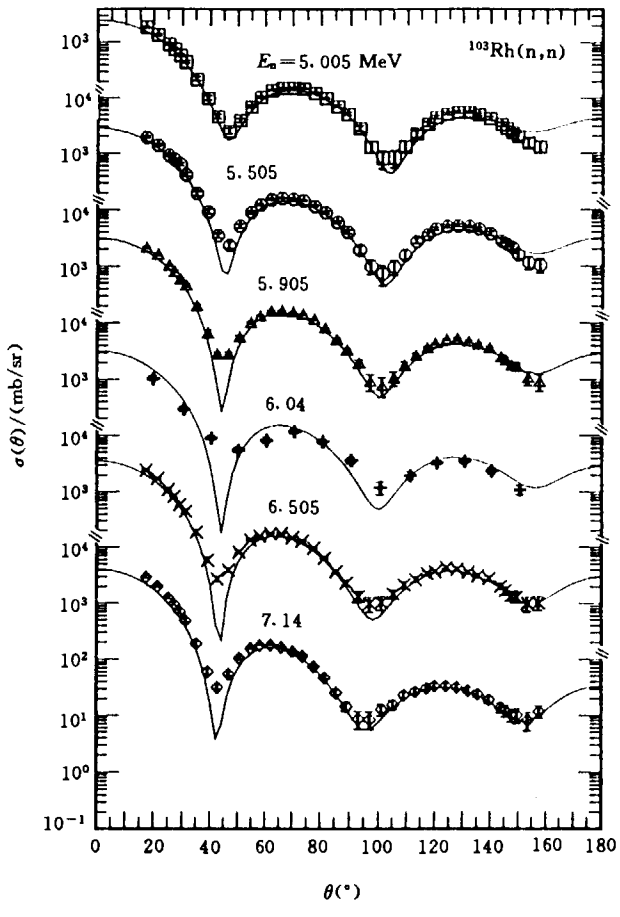

Fig. 2b The elastic scattering angular distribution

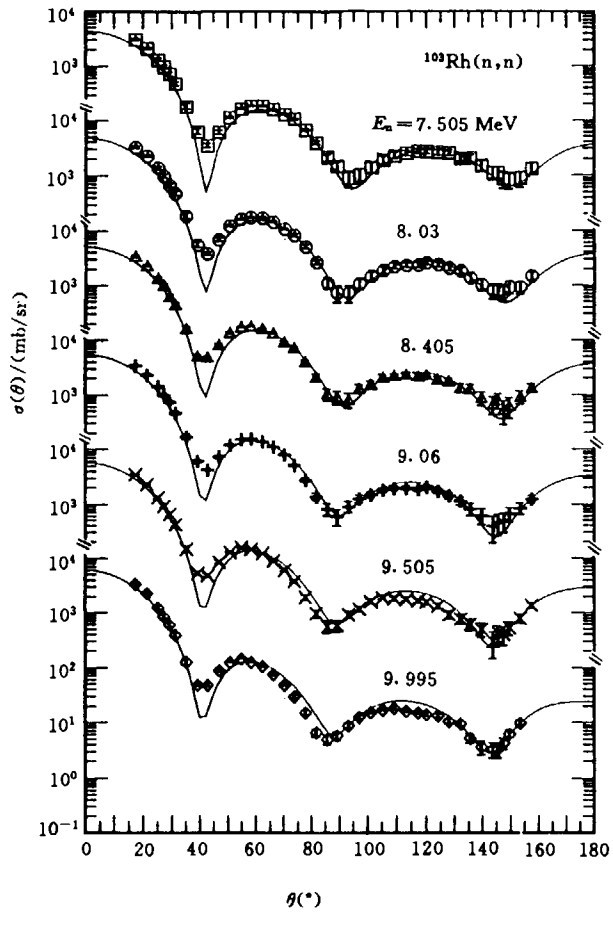

Fig. 2c The elastic scattering angular distribution

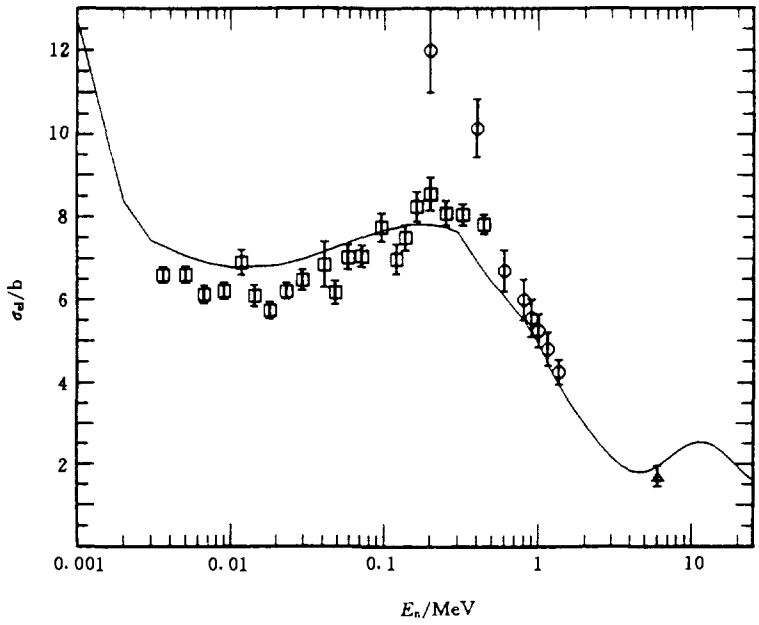

Fig. 3 The elastic scattering cross section

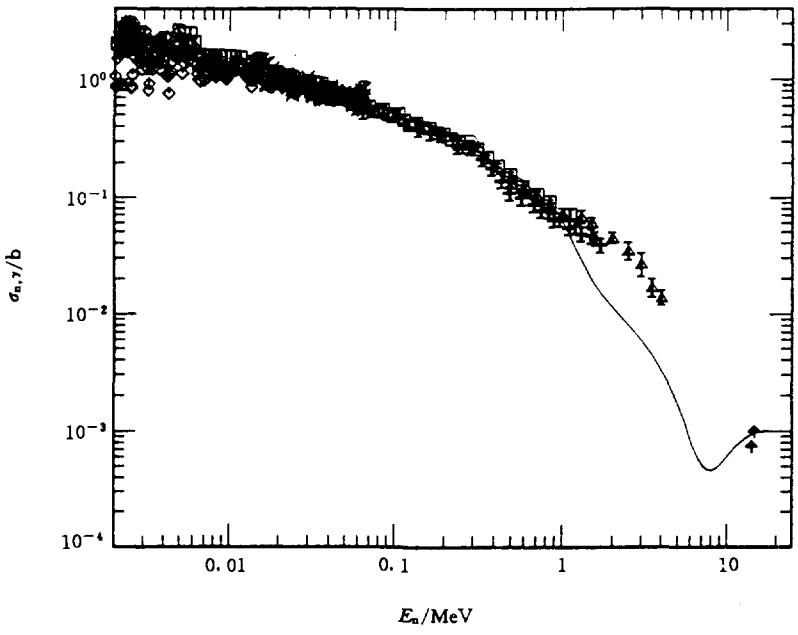

Fig. 4 The (n,γ) cross section

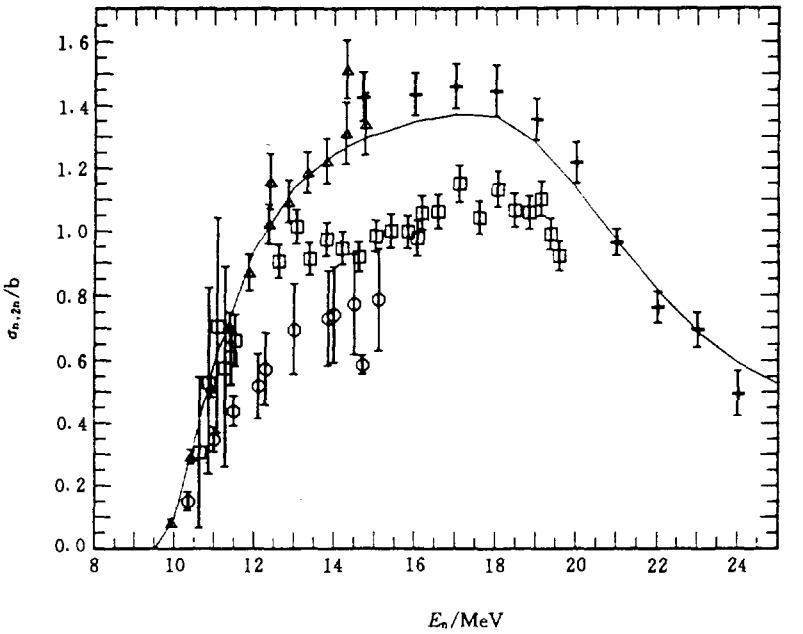

Fig. 5 The (n,2n) cross section

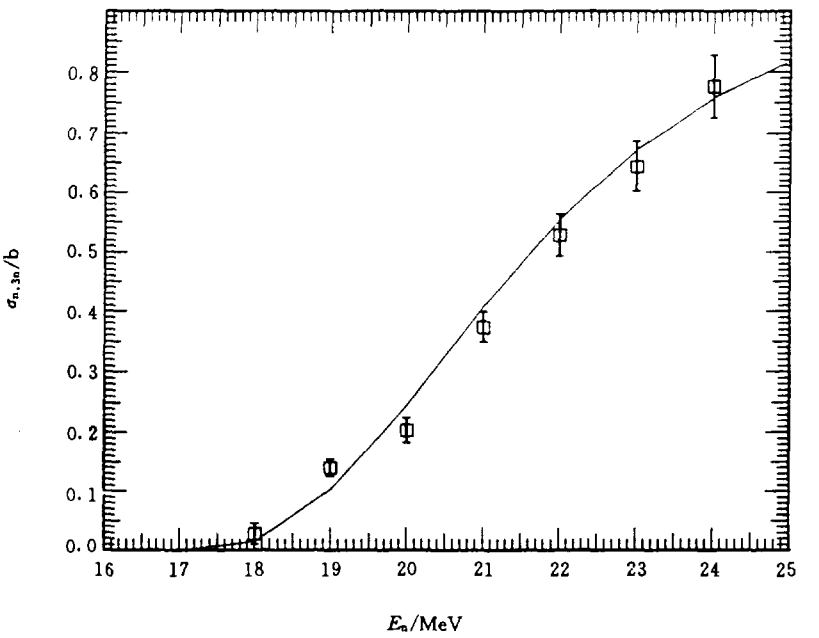

Fig. 6 The (n,3n) cross section

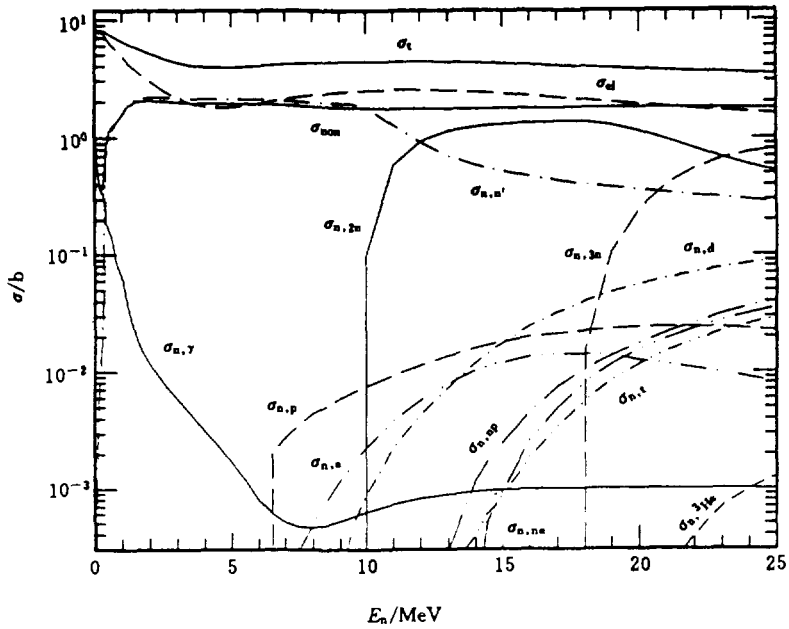

Fig. 7 The cross section of n+^{103}Rh reaction

References

[1] Shen Qingbiao, Commun. Nucl. Data Progress, 7, 43(1992)

[2] P. D. Kunz, "Distorted Wave Code DWUCK4", University of Colorado

[3] Zhang Jingshang, Private Communication

[4] Su Zongdi et al., Commun. Nucl. Data Progress, 12, 83(1994)

[5] Su Zongdi et al., Chin. J. Nucl. Phys., 8, 149(1986); INC(CPR)-2, 1986

[6] F. Rigaud et al., Nucl. Phys., A173, 551(1971)

[7] F. Rigaud et al., Nucl. Science & Engineering, 55, 17(1974)

[8] Poentz, Neutron Cross Section of Fission Product Nuclei, 85(1979)

[9] Frehaut et al., Neutron Cross Section at 10~50 MeV Brookhaven 399(1980)

[10] L. R. Veeser et al., Phys. Rev., C16, 1792(1972)

[11] A. Paulsen et al., Z. Phys., 238, 23(1970)

[12] Tewes et al., UCRL-6028-T 1960

[13] Lu Wen-deh et al., Phys. Rev., C1, 358(1970)

[14] L. Husain et al., J. of Inorganic and Nuclear Chemistry, 30, 3145(1968)

[15] J. Csikai et al., Nucl. Phys., 41, 316(1963)

CN9701143

III DATA EVALUATION

Evaluation of H Total Neutron Cross Section from 20 MeV to 2 GeV

Liu Tingjin

(China Nuclear Data Center, CIAE)

Introduction

The nuclear data in intermediate and high energy region have been widely used in various fields for last ten years, such as radioactive waste processing, radio therapy for cancer etc. So the measurements and evaluations of these data become more and more, these require the standard cross section in this energy region, just like already did in low energy region ($<$20 MeV).

In this work, the H total neutron cross section was evaluated from 20 MeV to 2 GeV, the purpose is to provide a cross section standard.

1 Experimental Data Evaluation

The H total neutron cross section was evaluated in the energy region from 20 to 2000 MeV. The 39 sets of experimental data were collected from EXFOR Experimental Data Library, CINDA, INIS index and most recent reports. The data were analyzed, evaluated, compared and processed, and as a result, the 11 sets of more reliable data[1~11] were selected, their uncertainties are small. The information and processing of them are listed in Table 1.

In summary, this evaluation was based on those data :

1) Measured later than 1960;

2) With liquid H, polyethylene or water as sample;

3) With white–light neutron source and time–of–flight method, or telescope detector;

4) With better incident neutron energy resolution ($\Delta E_n < 10\%$);

5) With smaller cross section uncertainty ($\Delta\sigma < 5\%$);

6) Necessary corrections were made.

On the contrary, the data were abandoned, for which the measurements were completed earlier than 1960, with H gas sample, threshold detector, larger ΔE_n and $\Delta\sigma$, or no detail information.

2 Data Fitting

The evaluated experimental data were fitted by using spline fit program SPF with knot optimization[12]. The number of input knots is 10, and the width for each sets of data is 0.0001. After 3 times of iteration, the fit values were obtained with 13 knots and reduced $\chi^2 = 0.993$. The fit values are taken as recommended data, shown in Fig. 1.

3 Data Covariance Evaluation

The most important and difficult thing is to give out the covariance matrix for the recommended values. It depends on the statistical and systematical errors of the experimental data.

First of all, the total and systematical errors were determined for each set of data after analyzing and evaluating, see Table 1.

Because there are a lot of data points and the error propagates according to the statistical laws, and the width for each set of data was taken as very small, which means that the discrepancies among the different data sets are not taken into account in the spline fitting, the error of fit value calculated in the fitting was taken as statistical one for recommended value.

The systematical error depends on two factors. One of them is the systematical error independently determined above for each set of data. Another is the systematical differences among them in certain energy region. In order to show the differences clearly, the data sets, for which there are more energy points, were fitted separately and plotted with remainder experimental data points (Fig. 2).

The total systematical errors for evaluated data were determined in 7 energy regions, as given in Table 2. The energy region division and the total systematical error determination were made by experience according to the measurement energy region, the individual systematical error and the differences among the data sets, as explained in Table 2. The total systematical errors were also calculated semi–quantitatively for each energy region according to the assumption: the systematical errors of each set of data are independent and follow the statistical laws. The calculated results are basically consistent with ones given by experience above.

Using the statistical and systematical errors determined above, the explicit covariance matrix in ENDF / B–6 format were constructed by using code CMC[13]. To avoid too large order of the matrix and convenient to use, the energy points were reduced to 36 by averaging the energy points and the statistical errors over given energy region.

The uncertainties of the recommended values are listed in Table 3, they are increased from 0.56% to 1.44% from 20 MeV to 2 GeV. The correlation coefficients among the different energy intervals are 0.70～0.95.

4 Comparison with other Evaluated and Experimental Data

The data are compared with those from ENDF / B–6 (< 100 MeV), the differences are 0.5～2.0% from 20 to 40 MeV, the maximum at about 30 MeV, and almost the same in the energy region 40～100 MeV (Fig. 3). It should be pointed out that the data of ENDF / B–6 were based on the calculation with *R*–matrix at 26 MeV, with phase–shift theory at 30 MeV, and the average of both at 28 MeV. Our new evaluation is very close to the calculated data with *R*–matrix and CENDL–2, especially at 30 MeV, as listed in Table 4. The data also compared with other experimental data[14], they are in agreement within the data errors (Fig. 4).

5 Conclusion Remarks

H total neutron cross section was evaluated and recommended based on the experimental data measured in last tens years. The data are accurate, reliable and changed very smoothly, and the uncertainties are quite small (0.56%～1.44%), so it can be used as standard cross section in intermediate and high energy region for measurement and evaluation of nuclear data.

The data measured by T. J. Devlin[3] and P. W. Lisowski[6] show that there seems to be a small broad peak at about 650 MeV. Due to it need to be proved further experimentally and so far there is no evidence in theory, it was smoothed out in the recommended data, but it need to be paid attention in both experiment and theory.

Acknowledgements

The author would like to give the thanks to Prof. Conde for his encouraging to do the work, to Dr. Shen Qingbiao and Prof. Cai Dunjiu for their discussions on the work and offering some information and data, to Profs. Lu

Table 1 The status of selected experimental data

Auther Lab. (Ref.)	Facility source (MeV)	Sample	Method detector	Correction error—analysis (%)	Comment (%)
Davis, Univ. of Wiscossion[1]	Tandem, T(d,n) 20–27.5	Hexane graphite	Stilbene, γ—di—scrimination	D_2 in H_2, 0.2; scat.—in, 0.2–0.9; temp. effect, 0.3; backg.; count. losses.; total 1–2	Syst. error $(0.2^2+0.3^2)^{1/2}=0.36$
Brady, Univ. of California [2]	Iso. cycl., ^{7}Li(p,n), 25–60, $\Delta E=2$	Polyethylene graphite	TOF, 3 scint. telescopes	Backg., 0.05; scat.—in, 0.01; multi—scatt., 10; dead—time, 0.3; disp. of air, 0.2; ΔE_n, 0.02; isot. abun., 0.06; C / H, 0.3.; syst. 0.3	Data error in table ~0.8, sys. 0.3, total $(\sim 0.8^2+0.3^2)^{1/2}$
Devlin, Rutgers State Univ.[3]	Princenton Accel., 0.2–2.4 GeV, $\Delta E=30$	Liquid H_2	TOF, liquid and plastic scintilator	Monitor, 0.05 mb; all syst. 0.09; $\Delta\sigma$ in table 0.4–2.4	Given sys. too small, taken as 0.3, total $\sqrt{0.3^2+0.052}$
Kreisler, Univ. of Michigan[4]	Cyclotron, Be(p,n), 0.8–1.92 GeV	Liquid H_2	Ioni. calori. or all absor. spectr.	Length of sample, 0.25; density and remainder gass, 0.87	Total error in table ~3; sys. 0.91 in it.
Measday, Harvard Univ. [5]	Cyclotron, D(p,n), 88–151, $\Delta E_n=6$	Liquid H_2, C H chemical compound	Plastic scintilator	Sample quantification, <0.1; statistical error given in table, ~2	Sys. error, 1.0; total ~2.2
Lisowski, LANL[6]	Weapons research facility, 39–730, $\Delta E_n=3.5$	Polyethylene graphite	NE 110 plastic scintilator	Statistical error given in table 0.5–1.8; sys. 1.0	Only data $E_n<330$ taken, data $E_n>330$ discr. with others.
Keeler, Tri Univ. Meson Facility[7]	Fast neutron facility D(p,n)	Liquid H_2	TOF, scint. telescope	Solid angle, 0.14; inela. scatt., 0.01; quasi—elastic scatt.; sample, 0.8	Stat. in table 0.75–2.8, syst. taken as 0.8, aban. first point (error large)
Cierjacks, KFK[8]	Syn.—cycl. U(d,xn), white—light	Polyethylene, graphite.	TOF, NE—213 liquid scint.	Dead time, 1.5; sample, 0.2; stati. 0.1–1.0; subtract C O, 0.2–1.0	Total error 2 in table, take sys. as 1 in it.
Larson, BNL [9]	ORELA, Be block, 20–81	Liquid H_2, 0.8224 atom / b	TOF (80 m), NE 110 plastic scint.	Total error 3–30 in table	$E_n>34$ aban. (error large), take 1.0 as syst.
Bowen, Harwell[10]	Syn.—cycl., Al(p,n), 20–111.5	Polyethylene, carbon	TOF, ΔE ~ 3.5, Org. scint.	Coun. losses; pulse pile—up; backg.; multi—scatt. & impur., < 0.2; statis. in table, 2–5.9; syst. < 2	$E_n>38$ taken ($E_n<38$, error too large), aban. 49.9 point (too large)
Bol, Catholic Univ. of Louvain[11]	Cycltron, ^{7}Li (p,n), 87–725	Liqiid H_2	TOF, plastic scintilator	Background; scattering—in; statis. error given in table 0.7–0.9	No information about syst. error, 0.8 taken

Hanlin and Zhao Wenrong for their helpful discussions on determining the systematical error.

Table 2 The systematical error

E_n / MeV	20~35	35~60	60~100	100~200	200~500	500~1000	1000~2000
Δ_i / %	0.36 (Davis)	(1.0) (Lisowski)	1.0 (Lisowski)	1.0 (Lisowski)	1.0 (Lisowski)	1.0 (Lisowski)	
	1.0 (Larson)	1.8 (Bowen)	1.8 (Bowen)		0.8 (Keeler)		
	1.0 (Cierjacks)		(1.0) (Measdy)	1.0 (Measdy)	0.33 (Devlin)	0.33 (Devlin)	0.33 (Devlin)
	(0.3) (Brady)	0.3 (Brady)				0.91 (Kreisler)	0.91 (Kreisler)
	(0.8) (Bol)	0.8 (Bol)					
D / %	0~1.7	1.9~4.4	~3.2	~0	1.6~4.7	Maximum 1.8	3.6~7.3
Σ / %	0.5	0.6	0.8	0.8	0.9	1.1	1.4
Comments	5 sets basical consis., (min Δ_i=0.3)	3 sets consis. (min Δ_i=0.3), Bowen disc. Δ_i=1.8	2 sets consis. (Δ_i=1.0), Bowen disc. Δ_i=1.8	2 sets consis. (Δ_i=1.0)	2 sets consis. (min Δ_i=0.33), Keeler disc. Δ_i=0.8	3 sets basi. consis. (min Δ_i=0.33), broad peak ?	Mainly based on Devlin, Kreisler larger disc.

note :

1. Δ_i individual systematical error for each set of data
2. D difference among the different data sets
3. Σ total systematical error
4. The figure in parentheses only as reference value, few data points in the region

Table 3 The uncertainty of recommended H total cross section

E_n / MeV	Total (%)	System (%)	E_n / MeV	Total (%)	System (%)
20.0~25.0	0.59	0.50	200.0~250.0	0.91	0.90
25.0~30.0	0.56	0.50	250.0~350.0	0.92	0.90
30.0~35.0	0.60	0.50	350.0~450.0	0.93	0.90
35.0~40.0	0.73	0.60	450.0~500.0	0.92	0.90
40.0~45.0	0.71	0.60	500.0~550.0	1.11	1.10
45.0~50.0	0.69	0.60	550.0~800.0	1.12	1.10
50.0~55.0	0.67	0.60	800.0~900.0	1.13	1.10
55.0~60.0	0.65	0.60	900.0~1000.0	1.12	1.10
60.0~85.0	0.83	0.80	1000.0~1500.0	1.42	1.40
85.0~200.0	0.82	0.80	1500.0~2000.0	1.44	1.40

Table 4 Comparison with ENDF / B–6 data and others

E_n / MeV	Present	ENDF / B–6	B–6 (R–M)	B–6 (P–S)	CENDL–2	JENDL–3
20.0	0.47918	0.48230			0.48170	0.482026
26.0	0.36860	0.36347	0.36345	0.36029	0.36348	
27.0	0.35345	0.34813	0.34859		0.34868	
28.0	0.33913	0.33297	0.33488	0.33104	0.33492	
29.0	0.32562	0.31893	0.32227		0.32208	
30.0	0.31288	0.30569	0.31080	0.30567	0.31011	

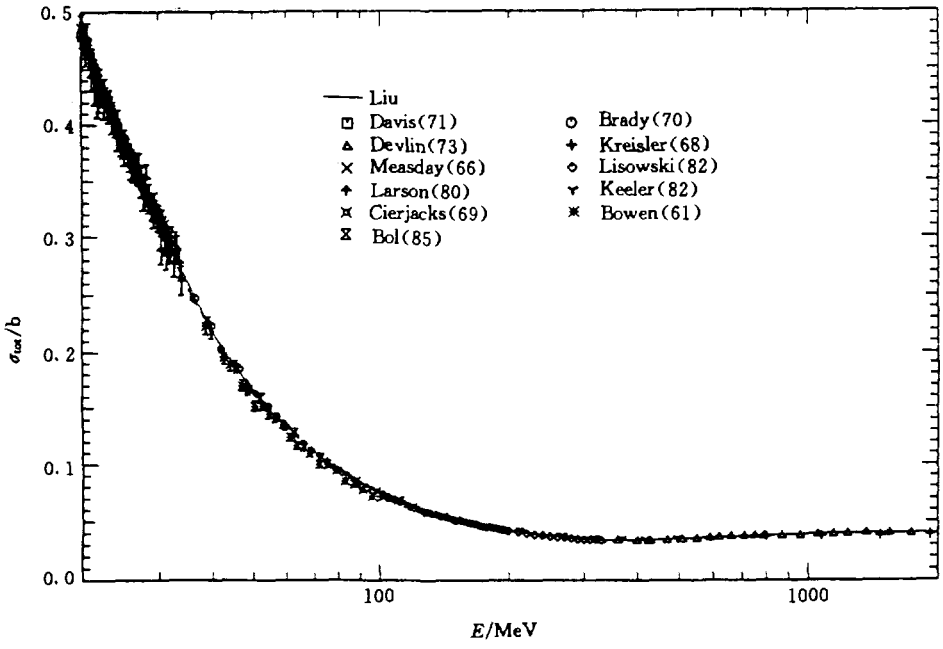

Fig. 1 H total neutron cross section

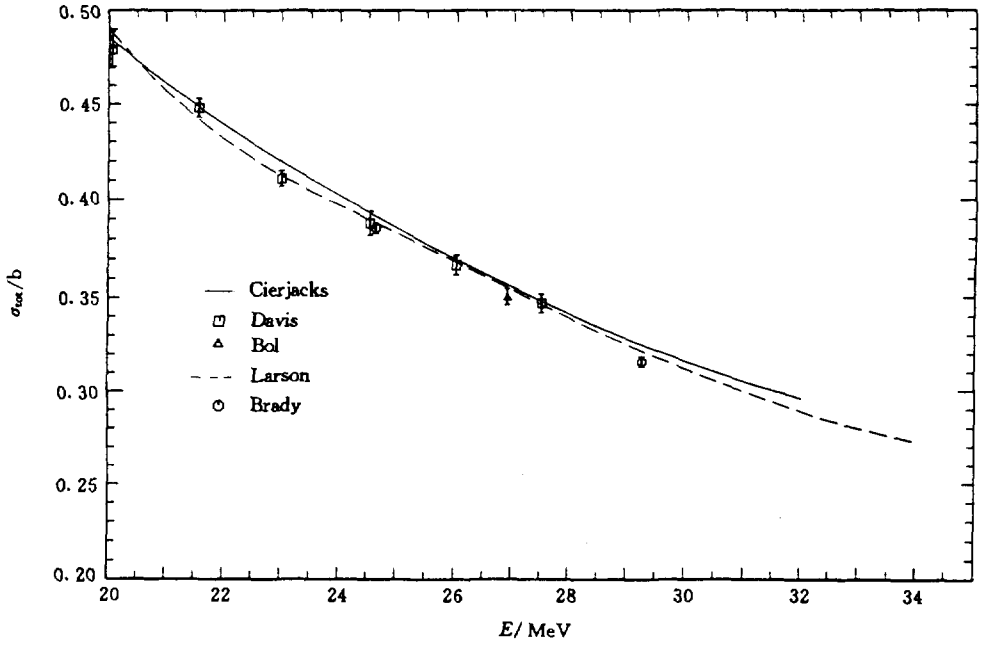

Fig. 2.1 The systematical differences of data sets

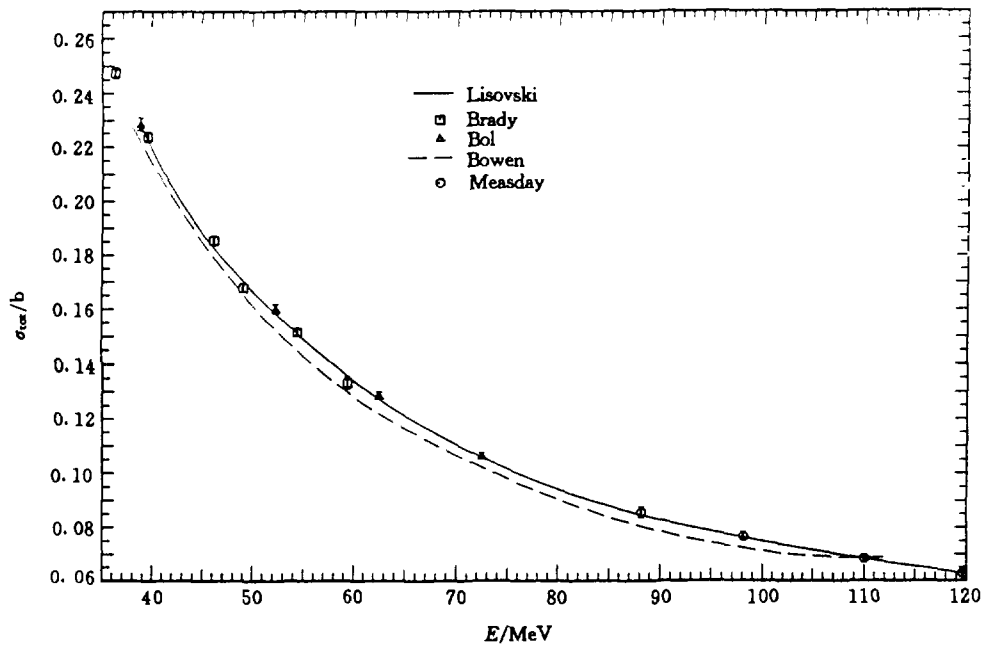

Fig. 2.2 The systematical differences of each data sets

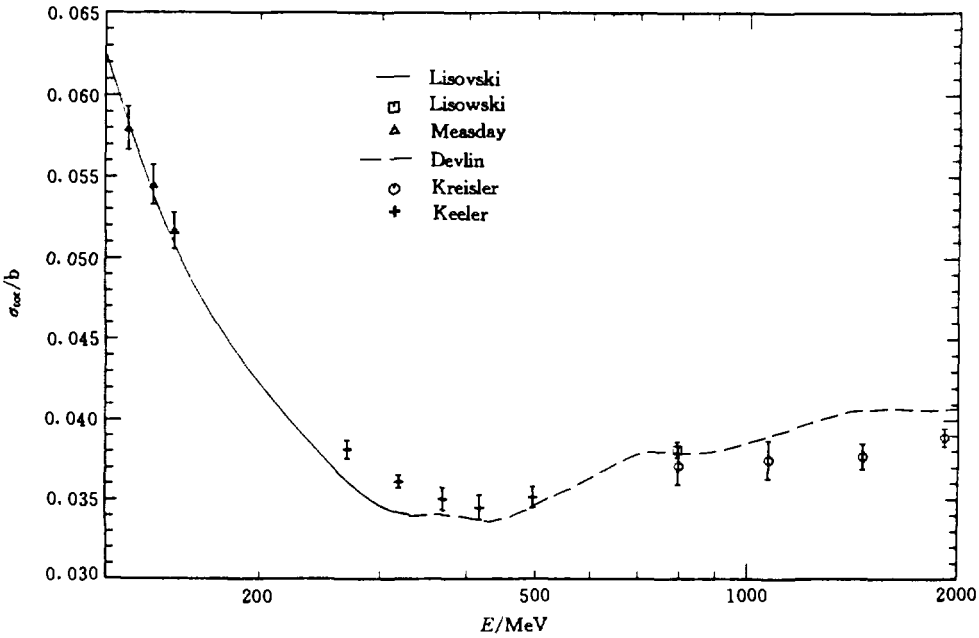

Fig. 2.3 The systematical differences of data sets

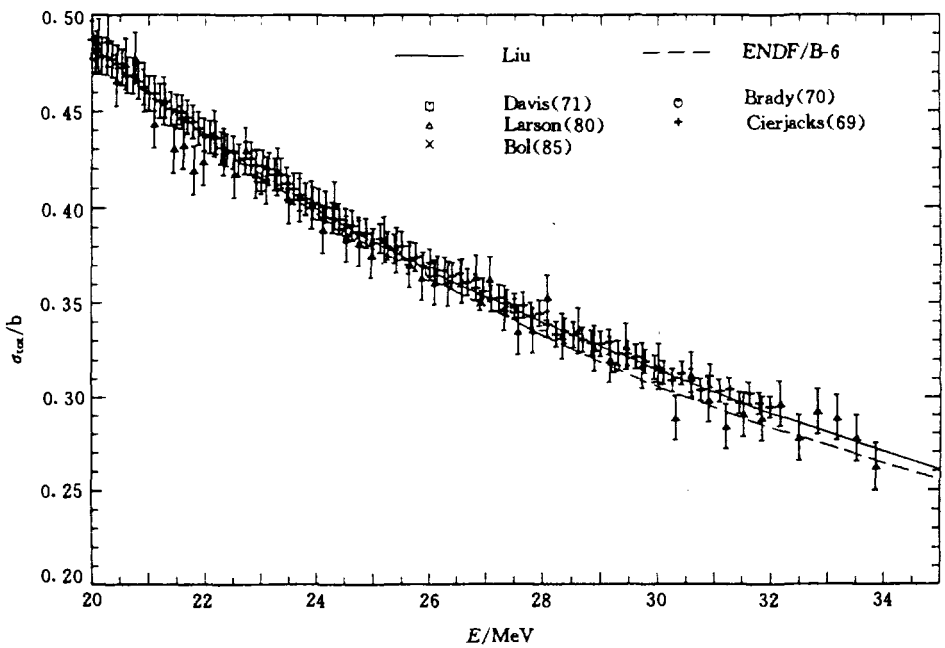

Fig. 3.1 The comparison between present evaluation and ENDF / B-6 (20~35 MeV)

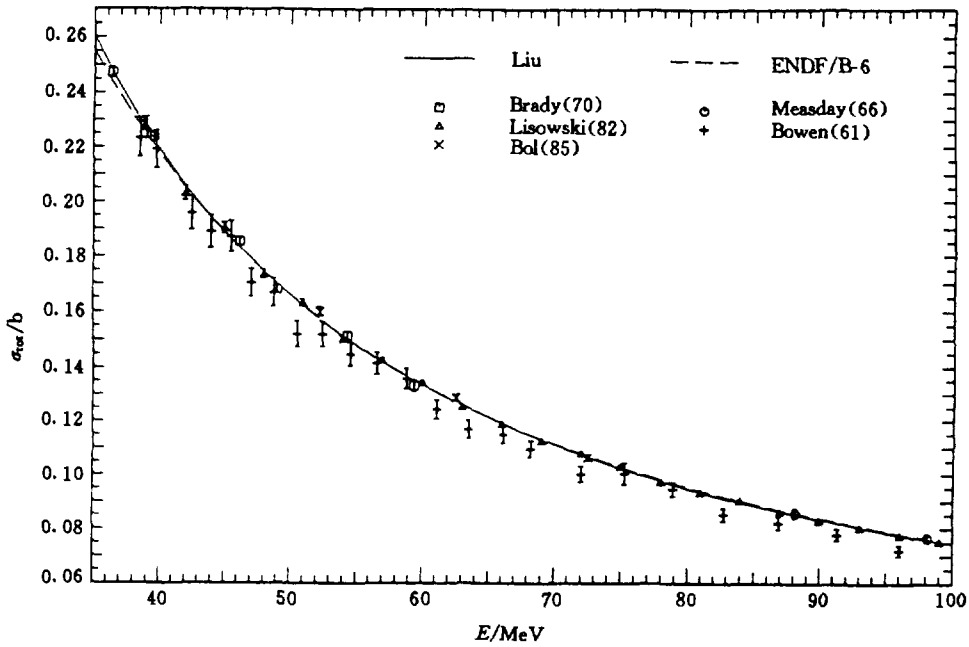

Fig. 3.2 The comparison between present evaluation and ENDF / B–6 (35～100 MeV)

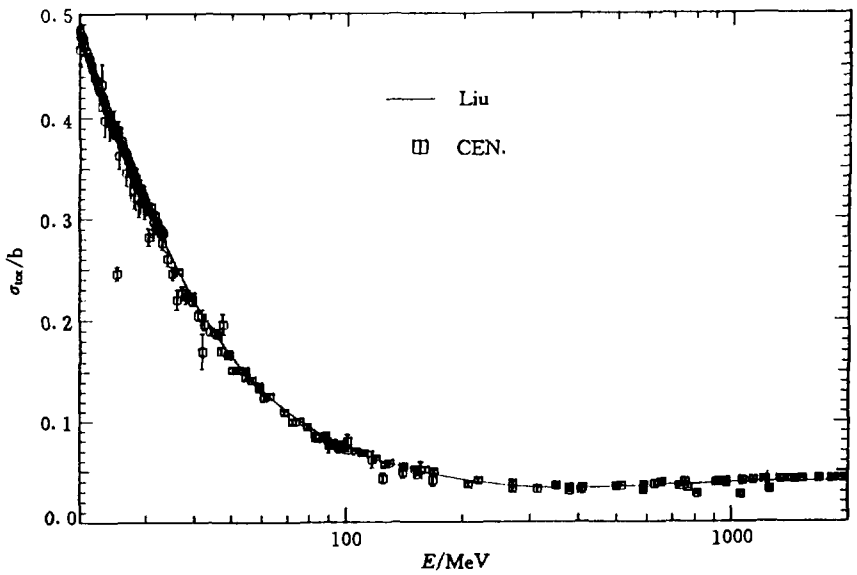

Fig. 4 The comparison between present evaluation and CEN data

References

[1] J. C. Davis et al., PR / C, 3, 1798(1971)
[2] F. P. Brady et al., PRL, 25, 1628(1970)
[3] T. J. Devlin et al., PR / D, 8, 136(1973)
[4] M. N. Kreisler et al., PRL, 20, 468(1968)
[5] D. F. Measday et al., NP, 85, 142(1966)
[6] P. W. Lisowski et al., PRL, 49, 255(1982)
[7] R. K. Keeler et al., NP / A, 377, 529(1982)
[8] S. Cierjacks et al., PRL, 23, 866(1969)
[9] P. H. Bowen et al., NP, 22, 640(1961)
[10] D. L. Larson et al., ORNL–5787, 174(1980)
[11] A. Bol et al., PR / C, 32, 623(1985)
[12] Liu Tingjin et al., CNDP, 11, 116(1994)
[13] Liu Tingjin, internal report (1990)
[14] R. K. Jung, (Norwood, Massachusetts 02062, USA), Private Comm. (1991)

CN9701144

The Evaluation and Calculation of Production Cross Sections for ^{11}C, ^{13}N and ^{15}O from ^{11}B, ^{13}C, $^{15}N(p,n)$ and $^{16}O(p,x)^{13}N$ Reactions up to 80 MeV

Zhuang Youxiang

(China Nuclear Data Center, CIAE)

Introduction

The medical radioisotopes are used for diagnostic and therapeutic purposes, as well as metabolism and physiological function researches in modern medicine. If a short–lived radioisotope emits a predominant or single γ–rays of 60~ 300 keV, it is of greater advantage since single photon emission computed tomograph (SPECT) can be performed; similarly β^+ emitters are also of great significance since three dimensional high resolution scans can be obtained via

positron emission tomography (PET). Some of the radioisotopes find therapeutic applications, especially if they emit α or high energy β^- particles, or Auger electrons [1].

The major applications are of functional imaging using PET agents for ^{11}C, ^{13}N and ^{15}O.

Nuclear data relevant to medically important radioisotopes can be divided into two major categories : the nuclear decay data and nuclear reaction cross sections. The former is of prime importance in deciding upon the suitability of a radioisotope for medical application, and the latter is of great significance regarding the production and radionuclidic quality control of the desired radioisotope. In general, the nuclear decay data are known with sufficient accuracies, but the reaction cross section needs to pay more attention, especially charged particle nuclear data (CPND), because they are scarce and scattered.

1 The Evaluations of Experimental Data and Theoretical Calculations

1.1 General Analysis

The related data measured before 1995 were collected. The bibliography and index to CPND are as follows:

Nuclear Science Abstracts; Nuclear Data Table; Atomic Data and Nuclear Data Table; INIS Atomindex; UCRL–50400, BNL–NCS–50640, 51771; EXFOR Master–File Index.

The excitation functions of ^{11}B, ^{13}C, $^{15}N(p,n)$ and $^{16}O,(p,\alpha)$ reactions were measured with the aid of either residual nucleus activity or outgoing neutron methods. Enriched sample, stacked target, separate monitor–foil, NaI(Tl) crystal, plastic scintillator, Ge–Li detector, BF_3 neutron counter, as well as beam current integration, chemical separation, coincidence technique etc. were used in these measurements.

In general, there are some experimental data in energy range from threshold to 30 MeV, thus it is necessary for each reaction to do theoretical calculation for interpolation or / and extrapolation of experimental data up to 80 MeV.

(1) $^{11}B(p,n)^{11}C$ Reaction Cross Section

The main 9 measurements are listed in Table 1.

Table 1 The main measurements of $^{11}B(p,n)^{11}C$ reaction cross section

Author (y)	Lab	Energy range / MeV
N. M. Hintz (1952)[2]	1USAHRV	0.2~99
J. H. Gibbons (1959)[3]	1USAORL	2.9~5.5
M. Furukawa (1960)[4]	2JPNTOK	4.7~15
G. Albouy (1962)[5]	2FR PAR	36~150
L. Valentin (1963)[6]	2FR FR	150~160
L. Valentin (1965)[7]	2FR PAR	40~160
K. Ramavataram (1980)[8]	1CAN LUQ	3~6
B. Anders (1981)[9]	2GERHAM	11~28
S. M. Grimes (1985)[10]	1USALRL	16~26

All the experimental data are shown in Figs. 1~2, except an early data of Ref. [2]. They coincide with each other. Thus, the recommended values can be obtained from fitting experimental data.

(2) $^{13}C(p,n)^{13}N$ Reaction Cross Section

There are 5 measurements, see Table 2.

Table 2 The main measurements of $^{13}C(p,n)^{13}N$ reaction cross section

Author (y)	Lab	Energy range / MeV
J. H. Gibbons (1959)[11]	1USAORL	3.9~5.3
L. Valentin (1965)[12]	2FR PAR	150~160
E. Ramstrom (1979)[13]	2SWDSWR	3.2~4.3
S. W. Kittwanga (1989)[14]	2BLGBRU	5.2~30.6
M. L. Firouzbakht (1991)[15]	1USABNL	2.09~33.55

In Fig. 3, four sets of measured data are shown. The dispersion on these data of Ref. [14] is still remarkable, therefore the fitting curve is based on Refs. [11, 13] and [14].

(3) $^{16}O(p,\alpha)^{13}N$ Reaction Cross Section

Altogether 7 measurements from 1958 to 1989 were collected, they are listed in Table 3.

Table 3 The main measurements of $^{16}O(p,\alpha)^{13}N$ reaction cross section

Author (y)	Lab	Energy range / MeV
A. B. Whitehead (1958)[16]	1CANCAN	6.2~16
M. Furukawa (1960)[17]	2JPNTOK	9.7~15
L. Valentin (1963)[18]	2FR PAR	150~160
R. H. Mccamis (1973)[19]	1CANALA	6.5~7.7
W. Gruhle (1977)[20]	2GERKLN	6.7~9.3
M. Sajjad (1986)[21]	1USABNL	6.7~16
S. W. Kittwanga (1989)[22]	2BLGBRU	15.6~27.8

The experimental data are shown in Fig. 4. It is evident that the recommended values from threshold to 28 MeV can be obtained from fitting measured data.

(4) $^{15}N(p,n)^{15}O$ Reaction Cross Section

The 3 measurements collected up to 1995 are listed in Table 4 and shown in Fig. 5.

Table 4 The main measurements of $^{15}N(p,n)^{15}O$ reaction cross section

Author (y)	Lab	Energy range / MeV
K. Murphy (1981)[23]	1USADKE	5.5~9.3
M. Sajjad (1984)[24]	1USABNL	3.7~17
S. W. Kittwanga (1989)[25]	2BLGLVN	16~28

It is evident that theoretical calculation is indispensable to get the recommended values from 28 to 80 MeV.

1.2 Theoretical Calculation

The excitation functions of ^{13}C, $^{15}N(p,n)$ and $^{16}O(p,x)^{13}N$ reactions were calculated by the code ALICE95[26] up to 80 MeV. The evaporation calculations were performed according to the theory of Weisskopf and Ewing. The nuclear masses were calculated from the Meyers and Swiatecki mass formula, including shell corrections and pairing effects. The level density parameters were taken from the work of Ignatyuk. The inverse cross sections were calculated by using the optical model. The hybrid model was chosen for the pre–equilibrium reactions. The nucleon–nucleon mean free paths were used in these calculations.

The comparison between calculated cross sections of ^{13}C, $^{15}N(p,n)$ and $^{16}O(p,x)^{13}N$ reactions by code ALICE95 and experimental data from threshold to 80 MeV are given in Figs. 6~8.

2 Recommended Values and Their Errors

2.1 The recommended values for $^{11}B(p,n)^{11}C$ reaction cross section were based on experimental data from 2.574 to 155 MeV (see Fig. 1~2).

2.2 The recommended values for $^{13}C(p,n)^{13}N$ reaction cross section were based on experimental data between 3.2355~30.6 MeV (see Fig. 3) and taken from the smoothed calculated results from 30 to 80 MeV (see Fig. 6).

2.3 $^{16}O(p,x)^{13}N$ reaction can be produced from five different types, they are listed in Table 5.

Table 5 $^{16}O(p,x)^{13}N$ reaction types, Q values and threshold energies

Reaction	$^{16}O(p,\alpha)$	$^{16}O(p,pt)$	$^{16}O(p,^3He)$	$^{16}O(p,\alpha d)$	$^{16}O(p,2n2p)$
Q value / MeV	−5.218	−25.033	−25.797	−29.100	−33.515
Thres. Energy / MeV	5.547	26.60	27.41	30.92	35.61

The recommended values for $^{16}O(p,x)^{13}N$ reaction cross section were based on the experimental data for $^{16}O(p,\alpha)^{13}N$ reaction between 5.547~27.0 MeV (see Fig. 4), because the other four reaction channels have not been opened; and taken from the shape of theoretical calculation between 27~80 MeV (see Fig. 7).

2.4 The recommended values for $^{15}N(p,n)^{15}O$ reaction cross section were based on experimental data of Sajjad[24] and Kittwanga[25] et al. between 3.7~28 MeV (see Fig. 5), because they coincide with each other within their errors and link up one another, and the shape of theoretical calculation between 28~80 MeV (see Fig. 8).

The smallest cited errors for $^{11}B(p,n)^{11}C$, $^{13}C(p,n)^{13}N$, $^{16}O(p,x)^{13}N$ and $^{15}N(p,n)^{15}O$ reaction cross sections based on experiments are adopted 10% by this work, because almost all measurements with accuracies of 7%~12%; and the errors for the theoretical calculations are about 20%~30%.

Acknowledgement

This work is supported by the International Atomic Energy Agency (IAEA).

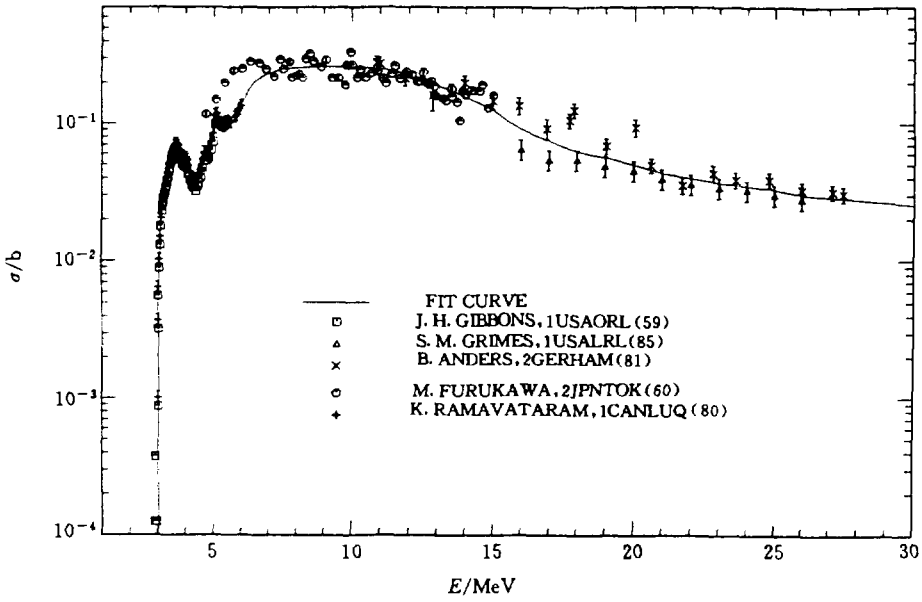

Fig. 1 $^{11}B(p,n)^{11}C$ reaction cross section for threshold ~30.0 MeV

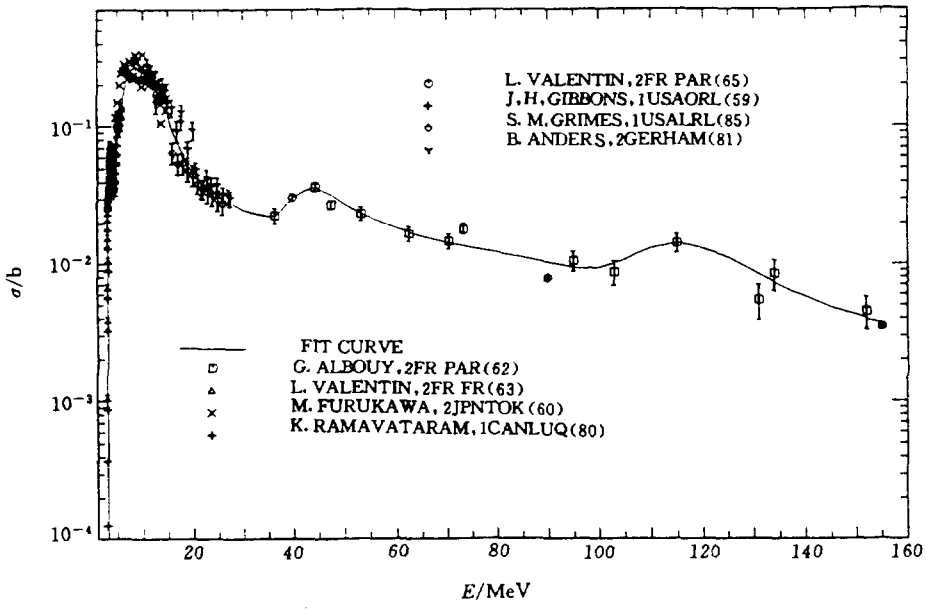

Fig. 2 $^{11}B(p,n)^{11}C$ reaction cross section for threshold ~155 MeV

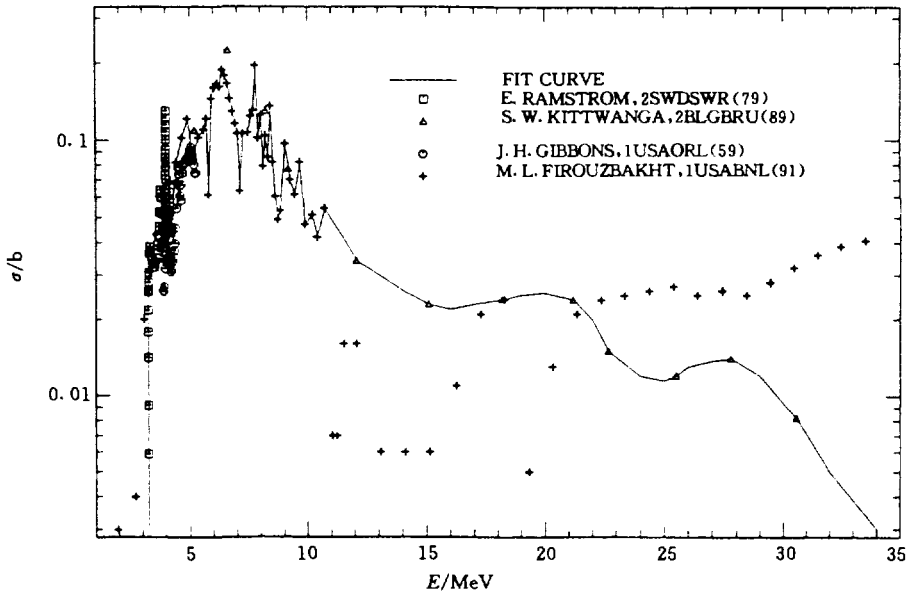

Fig. 3 $^{13}C(p,n)^{13}N$ reaction cross section for threshold ~ 34 MeV

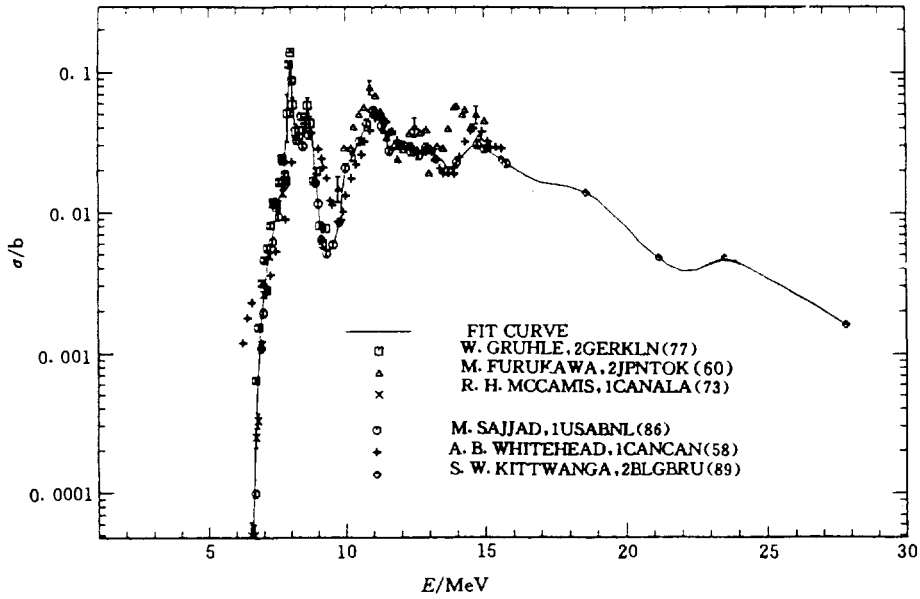

Fig. 4 $^{16}O(p,\alpha)^{13}N$ reaction cross section for threshold ~ 28 MeV

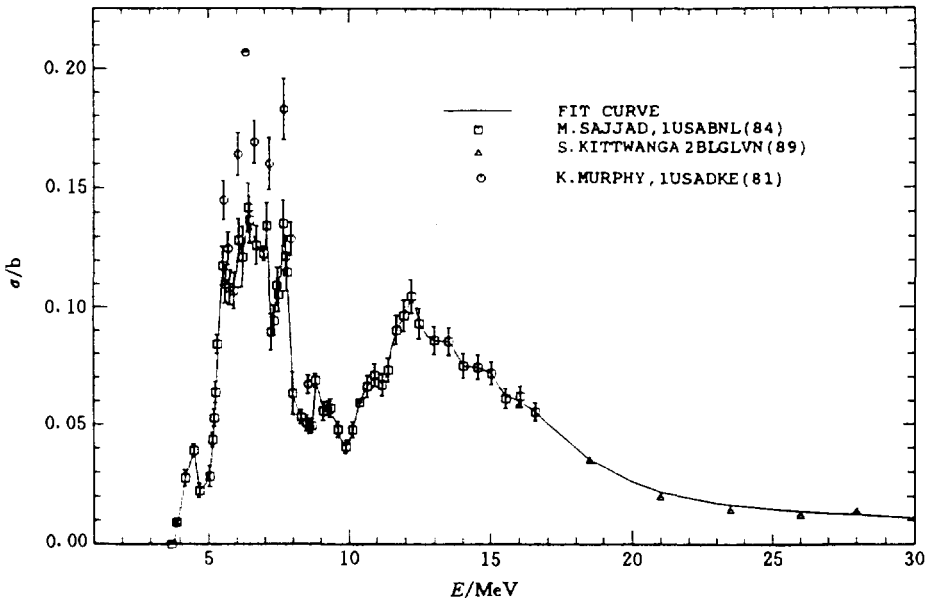

Fig. 5 $^{15}N(p,n)^{15}O$ reaction cross section for threshold ~28 MeV

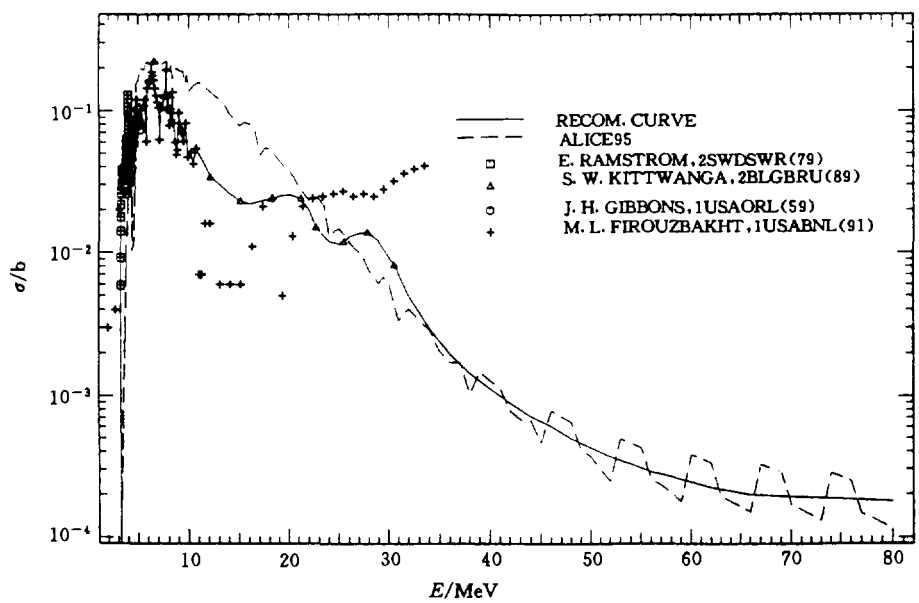

Fig. 6 Comparison of $^{13}C(p,n)^{13}N$ reaction cross section calculated by code ALICE95 with exp. data

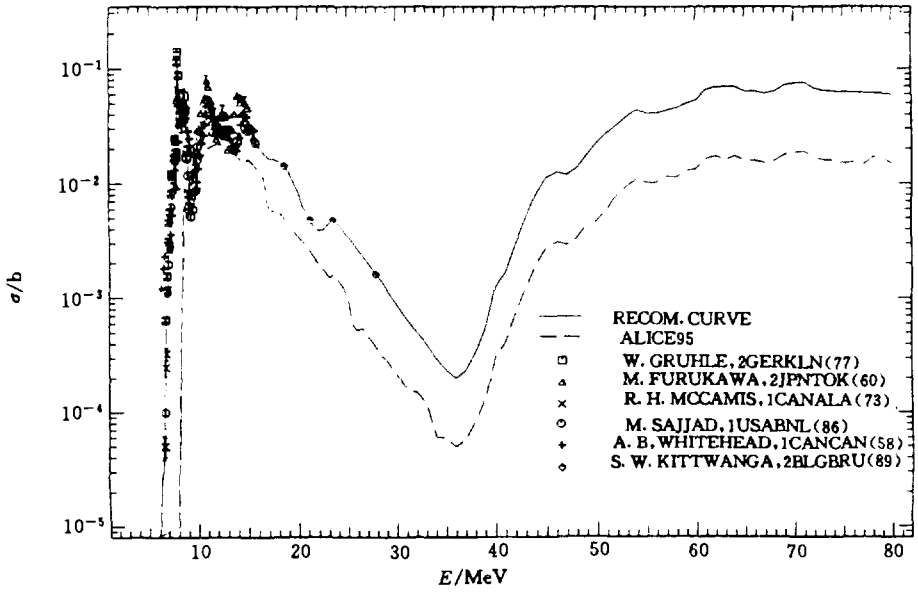

Fig. 7 Comparison of $^{16}O(p,x)^{13}N$ reaction cross section calculated by code ALICE95 with exp. data

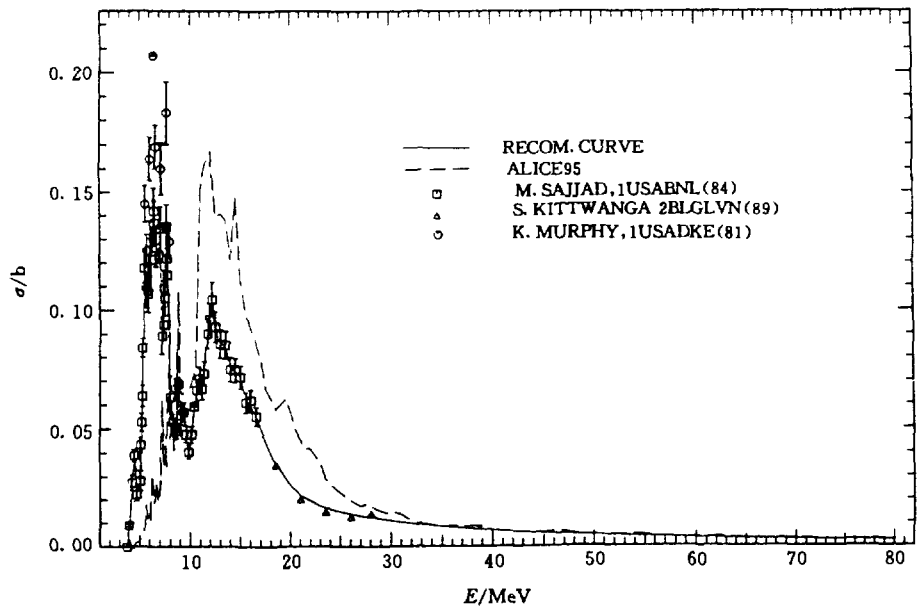

Fig. 8 Comparison of $^{15}N(p,n)^{15}O$ reaction cross section calculated by code ALICE95 with exp. data

References

[1] S. M. Qaim, INDC(NDS)−195 / GZ, p. 25~32(1987)
[2] N. M. Hintz et al., PR, 88, 19(1952)
[3] J. H. Gibbons et al., PR, 114, 571(1959)
[4] M. Furukawa et al., JPJ, 15, 2167(1960)
[5] G. Albouy et al., JPR, 23, 1000(1962)
[6] L. Valentin et al., PL, 7, 163(1963)
[7] L. Valentin et al., NP, 62, 81(1965)
[8] K. Ramavataram et al., Nuovo Cimento, A58, 342(1980)
[9] B. Anders et al., ZP / A, 301, 353(1981)
[10] S. M. Grimes et al., PR / C31, 1679(1985)
[11] J. H. Gibbons et al. PR, 114, 571(1959)
[12] L. Valentin et al., NP, 62, 81(1965)
[13] E. Ramstrom et al., NFL−6 (1979)
[14] S. W. Kittwanga et al., PR / C40, 35(1989)
[15] M. L. Firouzbakht et al., Radi. Acta, 55(1991)
[16] A. B. Whitehead et al., CTP, 36, 1276(1958)
[17] M. Furukawa et al., JPJ, 15, 2167(1960)
[18] L. Valentin et al., PL, 7, 163(1963)
[19] R. H. Mccamis et al., CJP, 51, 1689(1973)
[20] W. Gruhle et al., NP / A, 286, 523(1977)
[21] M. Sajjad et al., RCA, 39, 165(1986)
[22] S. W. Kittwanga et al., PR / C40, 35(1989)
[23] K. Murphy et al., NP, A335, 1(1981)
[24] M. Sajjad et al., Radiochim. Acta, 36, 165(1984)
[25] S. W. Kittawanga et al., PR / C42, 748(1990)
[26] M. Blann et al., Code ALICE / LIERMORE95

CN9701145

Evaluation of Cross Sections for Neutron Monitor Reactions $^{169}Tm(n,xn)^{168,167,166,165}Tm$ from Threshold to 100 MeV

Yu Baosheng Shen Qingbiao Cai Dunjiu

(Chinese Nuclear Data Center, CIEA)

The cross sections for $^{169}Tm(n,xn)^{168,167,166,165}Tm$ reactions in intermediate energy region are useful for neutron field monitor, safety design consideration and material damage research for fusion material irradiation test and the radioactivities induced in components of accelerator.

The evaluation of activation cross sections of (n,2n) reaction for ^{169}Tm has been performed below 20 MeV. In our evaluation, the identification and correction have been made to the differences and discrepancies among the existing activation cross sections from different laboratories to obtain more accurate data. The theoretically calculated data are supplemented in high energy region. The cross sections for $^{169}Tm(n,xn)^{168,167,166,165}Tm$ reactions are recommended from threshold to 100 MeV.

1 Cross Section of $^{169}Tm(n,2n)^{168}Tm$ Reaction

The most of the activation cross sections for $^{169}Tm(n,2n)^{168}Tm$ reaction were measured in CIAE. The measurements and evaluation of activation cross sections have been under–way in CIAE for a long time. The new measured data could contribute to this evaluated work and modify the recommended data.

In order to eliminate the discrepancies among the existing activation cross sections, the background neutron yield depending on both the "gas–out" effect and D–D breakup neutron need to be determined and subtracted accurately. It is noted that both effects increase with the neutron energy and strongly depend on the threshold of the specific reaction. Therefore, the accurate experimental data have been obtained in some laboratories recently.

The activation cross section was evaluated based on experimental data of Zhao Wenrong[1] in CIAE from 12 to 19 MeV and other measured data. There are only several points of experimental data from threshold energy 8 MeV to 13

MeV. The experimental data from 8 to 13 MeV were measured by Frehaut[2] with liquid tank method related to the known cross sections of $^{238}U(n,f)$ reaction. There is a difference between the standard cross sections of $^{238}U(n,f)$ used in the measurement and recent new values. Now, the cross sections, especially in 11 to 12 MeV energy region, are more suitable after using the new normalized cross sections from ENDF / B–6 in this work. The new correct values supersede the earlier data. The previous evaluated data are modified. The cross sections have been evaluated below 20 MeV based on experimental data. In order to extend the energy up to 100 MeV, we also gave the new data including the evaluation of the cross sections for producing nuclei $^{167, 166, 165}Tm$ from $^{169}Tm(n,xn)$ reactions.

The measured neutron cross sections above 20 MeV are still insufficient because of difficulties in providing an intense monoenergetic neutron source at these energies. The pertinent calculated method has been provided[3]. A set of neutron optical potential parameters for ^{169}Tm in the energy region of 2~ 100 MeV was obtained using available experimental data. The required cross sections were predicted since the calculated results for many available reaction channels are in agreement with existing experimental data.

For the cross sections of $^{169}Tm(n,2n)^{168}Tm$ reaction, the calculated values close to the experimental data around 23 MeV. Therefore, the cross section was recommended on the basis of the evaluated experimental data below 23 MeV and theoretically calculated data from 23 to 100 MeV, see in Fig. 1.

2 Cross Sections of $^{169}Tm(n,xn)^{167, 166}Tm$ Reactions

The calculated values are slightly lower than evaluated experimental data for $^{169}Tm(n,3n)^{167}Tm$ and passed through the measured data of (n,4n) of Bayhurst[4] at 26 and 28 MeV respectively. Then, the calculated data for $^{169}Tm(n,3n)^{167}Tm$ reaction were renormalized to the evaluated values in order to obtain the recommended values. For the cross section of $^{169}Tm(n,4n)^{166}Tm$ reaction, the calculated data were recommended. The results for these reactions are shown in Fig. 2.

3 Cross Sections of $^{169}Tm(n,5n)^{165}Tm$ Reaction

The calculated data were recommended due to no experimental data.

All of recommended data of $^{169}Tm(n,xn)^{168, 167, 166, 165}Tm$ reactions from threshold to 100 MeV are shown in Fig. 3.

Acknowledgements

The authors are indebted to IAEA (International Atomic Energy Agency), CNNC (China National Nuclear Corporation) and CIAE for their supports, and thank to Drs. A. B. Pashchenko, T. Benson, O. Schwerer, Lu Hanlin and Zhao Wenrong for kind help and suggestions.

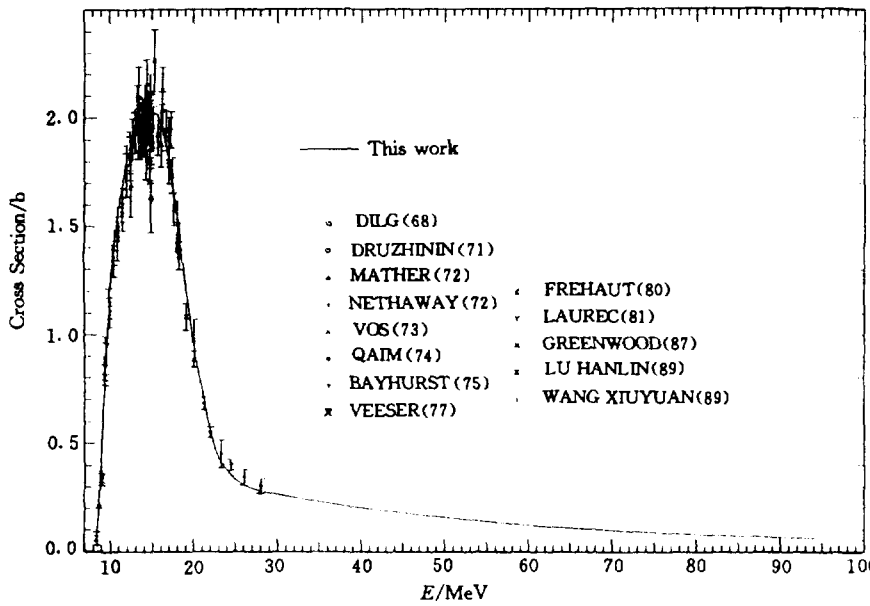

Fig. 1 Comparison of evaluated & measured data for $^{169}Tm(n,2n)^{168}Tm$ reaction

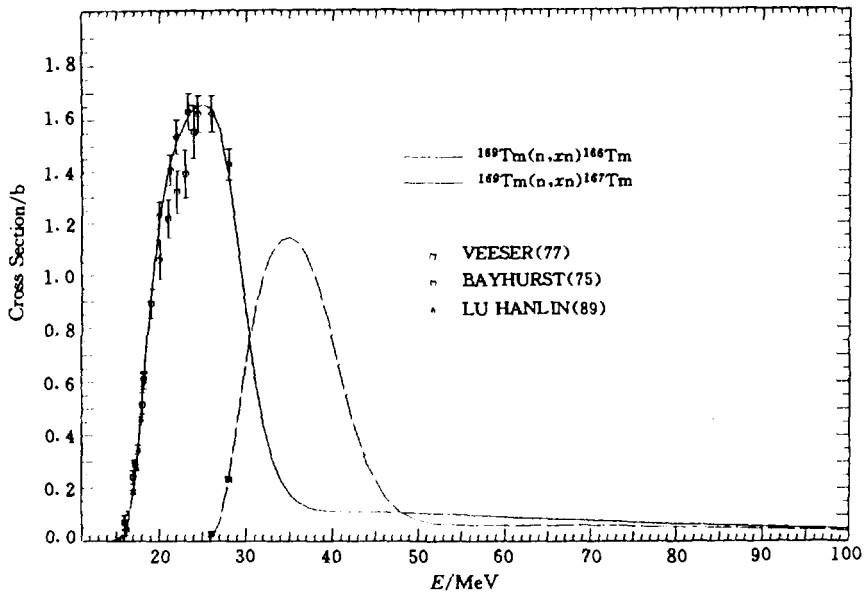

Fig. 2 Comparison of evaluated & measured data for $^{169}Tm(n,xn)^{167,166}Tm$ reactions

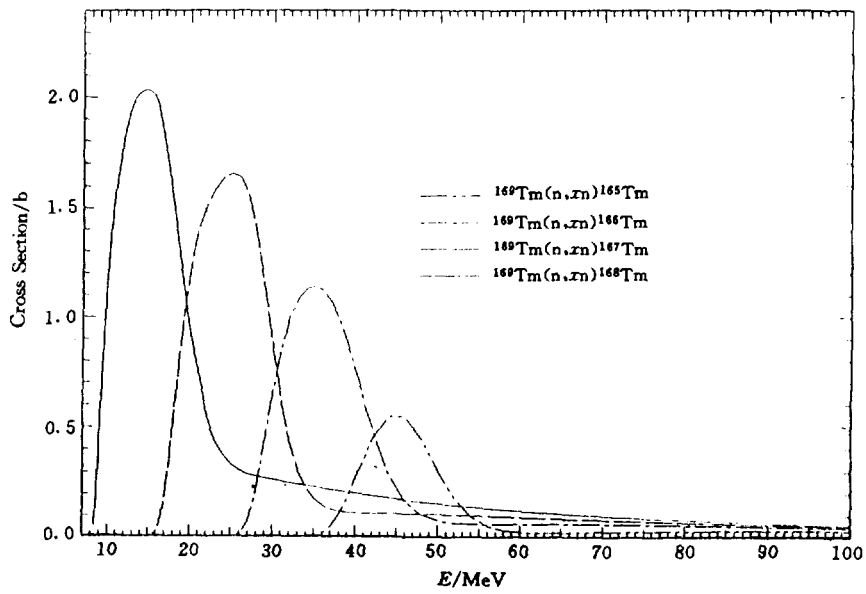

Fig. 3 Evaluated data for $^{169}Tm(n,xn)^{169,167\sim165}Tm$ reactions

References

[1] Zhao Wenrong et al., INDC(CPR)–16 (1989)

[2] J. Frehaut et al., Nuclear Cross Section and Tech., 425, 855(1975)

[3] Shen Qingbiao et al., This CPR work report (1995)

[4] B. P. Bayhurst et al., Phys. Rev., C, 12, 451(1975)

CN9701146

IV SYSTEMATICS RESEARCH

An Approach of a Systematical Description of Gamma–ray Spectra from (n,$x\gamma$) Reactions Induced by Fast Neutron

Fan Sheng Zhao Zhixiang

(China Nuclear Data Center, CIAE)

Abstract

Based on the semi–empirical method which used to calculate the gamma–ray production data from neutron induced reactions, within the target mass number of $20 < A < 220$, and incident neutron energy region of $E_n < 20$ MeV, the systematics for parameter R was obtained. And the sensitivity of the parameter R to the total spectra was studied.

Introduction

The gamma–ray production data from (n,$x\gamma$) reactions induced by incident fast neutrons, such as gamma–ray spectra and multiplicity, are very important for nuclear engineering application. And at present, stimulated by fusion research, demands are growing for detailed knowledge of photoproduction cross section and gamma–ray spectra of (n,$x\gamma$) reactions induced by up to 20 MeV. Although, in the course of the recent years, a great deal of reliable experimental data has been obtained for a wide nuclear mass range, it seems to be necessary, especially because of the experimental difficulty encountered, to seek also calculational method which can represent and provide the data required.

Recently, Zhao Zhixiang et al.[1] developed a semi–empirical method for calculation of continuum gamma–ray multiplicity and spectra from neutron induced reactions, which is based on the evaporation model. The semi–empirical method does not depend on the detailed knowledge of nuclear properties and allows to do separate calculation. In Zhao's work, only one parameter is

adopted, and the calculations are carried out with $C_T = 23.0$[1], which gives good agreements with measured gamma–ray spectrum.

However, Zhao's formulas also suffers from the fact that the gamma–ray emission probability from one level to another is simply to be proportional to the final energy level density, and do not consider the contribution of the pre–equilibrium of the particle emission in the total spectrum.

In the present work[2~4], within the target mass number of $20 < A < 220$ and incident neutron energy region of $E_n < 20$ MeV, a semi–empirical method based on evaporation model and exciton model is developed. In this work, the gamma–ray emission probability is considered to be proportional to the final energy level density and giant dipole resonance strength function. And two parameters k and R are adopted.

k can be got from a systematical formula[5] :

$$k = 0.035\ A\ \left(\ 1.0 + \frac{B_n}{E_n}\ \right)^3 \tag{1}$$

where A is the mass number, E_n and B_n are the incident neutron energy and neutron separation energy respectively.

Systematics for the parameter R was obtained by fitting measured data.

1 Systematics for R

In order to simplify the calculation, the level density is taken as the form of constant temperature

$$p\ (A,\varepsilon)\ \propto\ \exp\ (\ \varepsilon / T\ ) \tag{2}$$

where ε denotes the excitation energy, T is the nuclear temperature, and taken as[6, 7]

$$T = R\ \frac{13.0}{\sqrt{A}} \tag{3}$$

The Eq. (3) contains the mass number A and an adjustable parameter R. Using the semi–empirical formulas, the calculations for 12 targets including Ti, V, Cr, Fe, Zn, Ni, Nb, Mo, Ta, W, Au and Pb, were performed. The parameter R was adjusted to fit experimental total gamma–ray spectrum, see Figs. 1~4.

The values of parameter R obtained in fitting measured data, called local parameter, are listed in Table 1.

Table 1 The values of parameter R

	Ti	V	Cr	Fe	Zn	Nb	Mo	Ta	W	Au	Pb
R	3.0	2.9	2.9	2.96	2.8	3.0	2.6	2.0	2.0	1.8	2.0

The R can be described by a linear function

$$\bar{R} = a + b \times A \tag{4}$$

by using the least squares method, we have

$$a = 3.428$$
$$b = -0.00798$$

The $\bar{R}$ calculated by systematics Eq. (4) is called global parameter.

2 Sensitivity of the Parameter R

To estimate the uncertainties of the spectra predicted by the global parameter $\bar{R}$, the moments method was used and the variance of the global parameter $\bar{R}$ is obtained as follows :

$$V_{ar}(\bar{R}_i) = \bar{R}_i^2 M \tag{5}$$

$$M = \frac{1}{N} \sum_i t_i - \frac{1}{N(N-1)} \left(\sum_i t_i \right)^2 \tag{6}$$

$$t_i = \frac{\bar{R}_i - R_i}{R_i} \tag{7}$$

Based on Eq. (4) and the values of parameter R in Table 1, we get

$$M = 0.0034 \tag{8}$$

That means, the relative error of $\bar{R}$ is about 5%. The comparison of local parameter and the global parameter is given in Fig. 5. The local parameter is identical with the global parameter.

$S(R)$, the sensitivity of the parameter R to spectrum, is defined as follows :

$$S(R) = \frac{\partial f(R)}{f(R)\ \partial R} \tag{9}$$

where $f(R)$ is the total spectrum of (n,xy) reactions induced by neutron incident.

The sensitivities of the parameter R for Ti, Fe, Nb, Ta, Au to the total spectra were calculated and shown in Fig. 6.

3 Discussions

The results calculated with the local parameter and the global parameter in the semi–empirical method are in good agreement, and compared with those measured by Morgen et al.[8], see Fig. 3.

When the parameter R is varied, the change in the calculated results is small for Ti. It follows that the parameter R has a little effect to the curve's fashion, see Fig. 4.

The sensitivities of the parameter R for Ti, Fe, Nb, Ta, Au to the total spectra at the incident neutron energy 15.0 MeV are studied. It is found from the Fig. 6 that the sensitivities among the 5 nuclei are different, and the sensitivity of R to the total spectra is also small.

There are less measured data for ^{28}Si and no experimental data for ^{89}Y, however, the predictions of the systematics for parameter R are in agreement with the measured data of Drake et al.[11] and the results calculated by NDCP–1 code[11], see Figs. 7 and 8.

In a word, if no or less measured data available, the systematics for R can be simply and conveniently used to give prediction since only one parameter in this semi–empirical method.

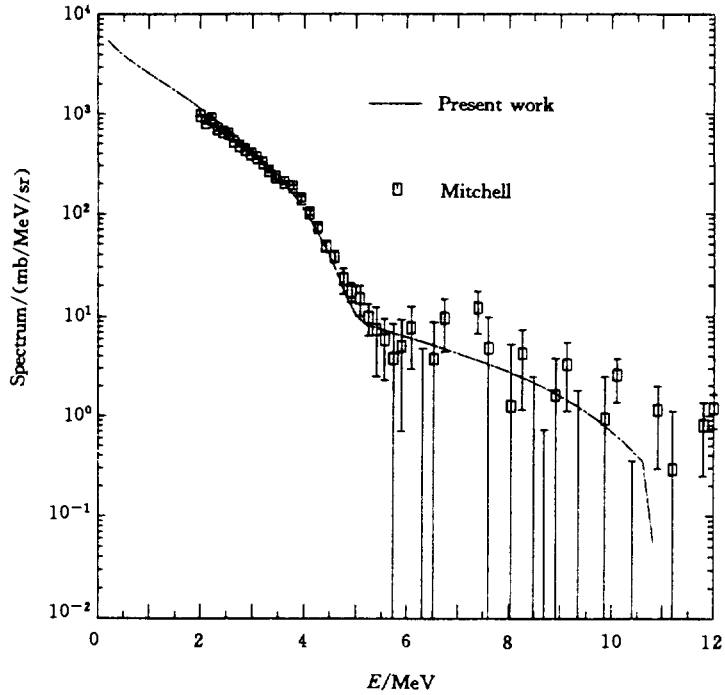

Fig. 1 Gamma spectrum for ^{181}Ta at $E_n = 5$ MeV

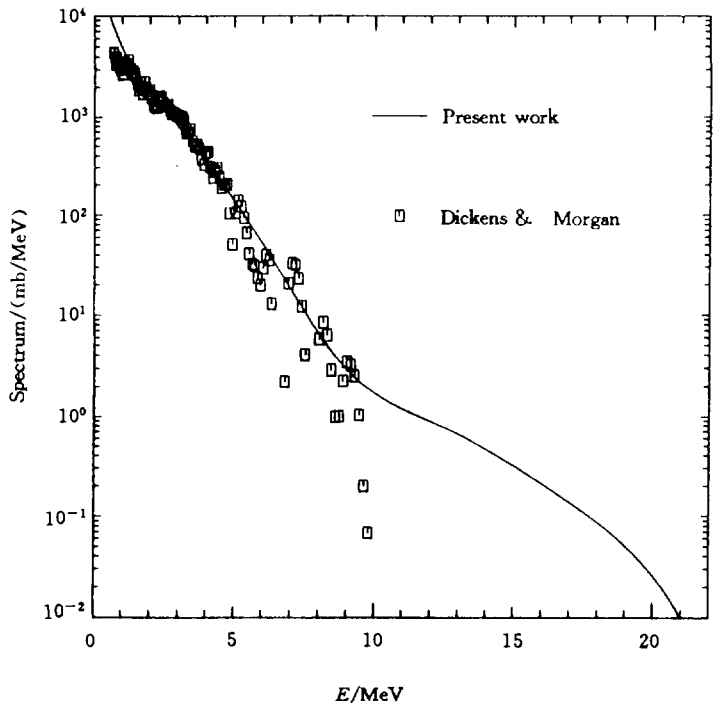

Fig. 2 Gamma spectrum for W at $E_n = 17$ MeV

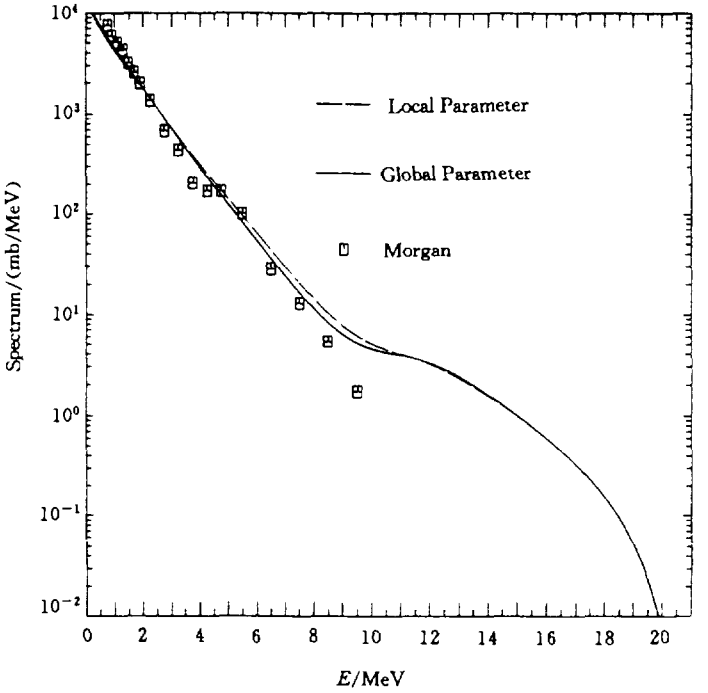

Fig. 3 Gamma spectrum for ^{197}Au at $E_n = 14$ MeV

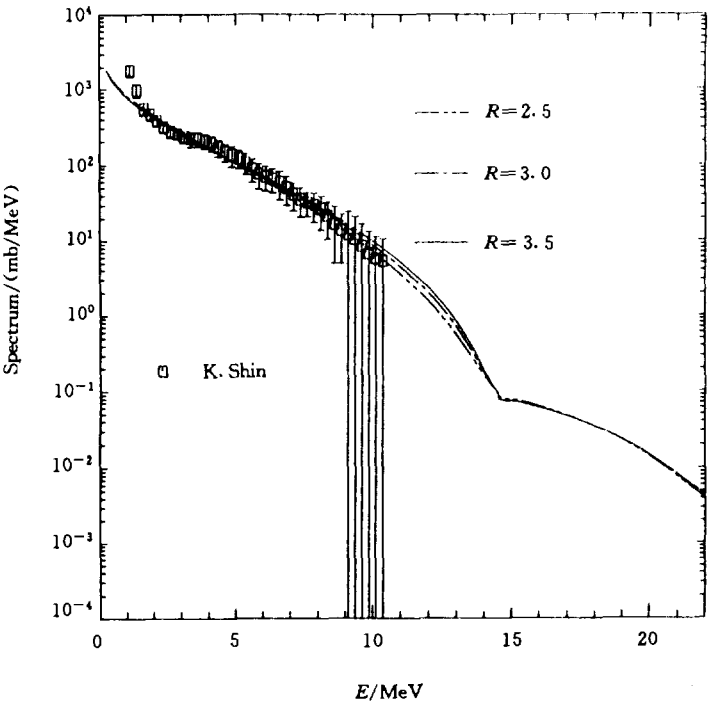

Fig. 4 Gamma spectrum for Ti at $E_n = 15$ MeV

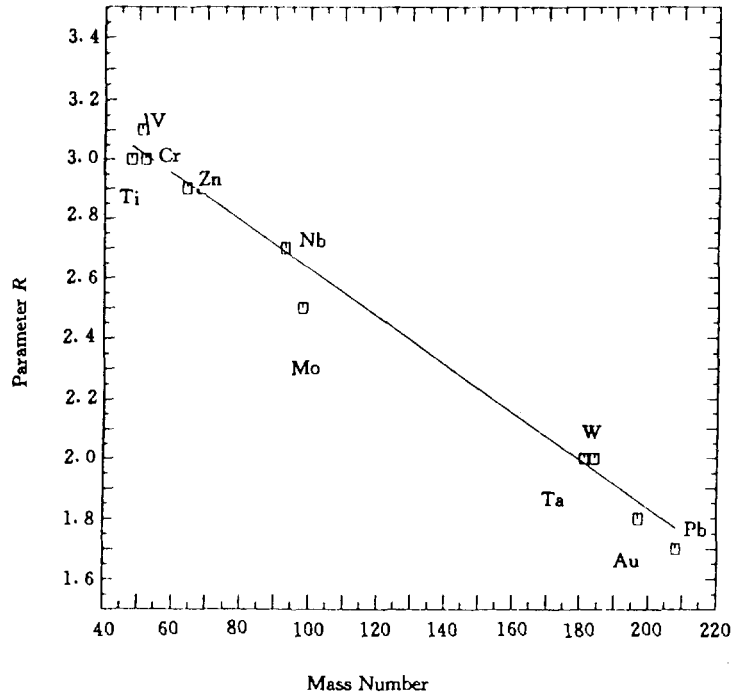

Fig. 5 Systematic analysis of parameter R

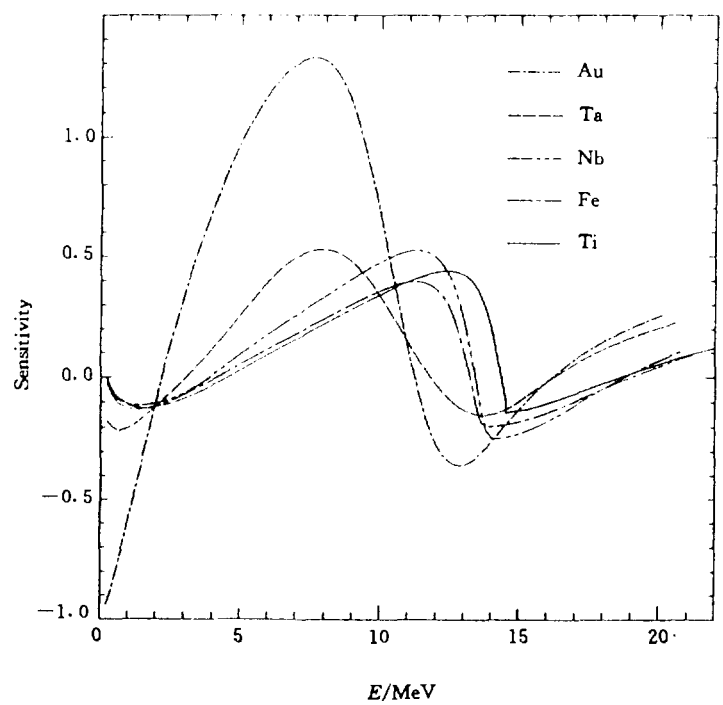

Fig.6 Sensitivity of spectrum to R

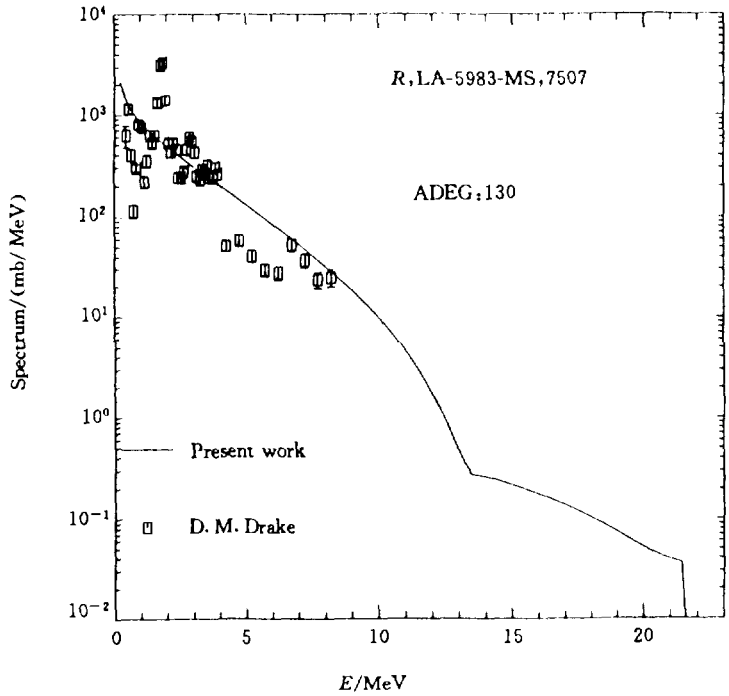

Fig. 7 Gamma spectrum for ^{28}Si at $E_n = 14.2$ MeV

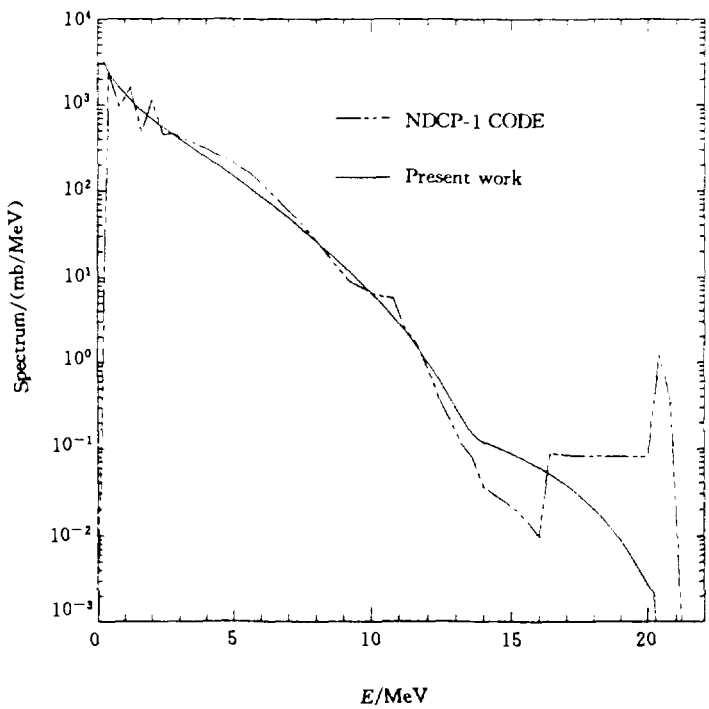

Fig. 8 Gamma spectrum for ^{89}Y at $E_n = 14$ MeV

References

[1] Zhao Zhixiang et al., Chin. J. Nucl. Phys., 17, 154(1995)

[2] Fan Sheng et al., to be published in Nucl. Sci. and Eng., 10(1996)

[3] Fan Sheng et al., to be published in Chin. J. Nucl. Phys., 2(1996)

[4] Fan Sheng et al., CNDP, 15, 71(1996)

[5] Zhao Zhixiang et al., Nucl. Sci. and Eng., 99: 367(1988)

[6] D. L. Livesey, Can. J. Phys., 33: 391(1955)

[7] G. Eder et al., Z. Phys., 253: 335(1972)

[8] G. L. Morgen et al., ORNL / TM–4973 (1975)

[9] K. Shin et al., Nucl. Sci. and Tech., 17, (7): 531(1980)

[10] D. M. Drake et al., Gamma–ray Production Cross Section for Fast Neutron Interactions with Several Elements 40, 284(1970)

[11] Liu Jianfeng et al., CNDP, 14, 8(1995)

V PARAMETER LIBRARY

Data File of Optical Model Parameter Sub–Library (CENPL–OMP)

Su Zongdi Sun Zhengjun
(China Nuclear Data Center, CIAE)

Yu Ziqiang Zuo Yixin
(Nankai University, Tianjin)

Wang Chenxiang
(China Institute of Atomic Energy)

Ma Gonggui
(Institute of Nuclear Science & Technology, Sichuan University)

Zhu Yaoyin Zhang Yujun
(Department of Physics, Jilin University)

Chen Zhenpeng
(Department of Modern Applied Physics, Tsinghua University)

Yao Lishan
(Department of Physics, Shaanxi Normal University)

The optical model is the most fundamental and important one in nuclear physics, and the optical model parameters (OMP) play a very crucial role in the nuclear model calculations of nuclear data and many theoretical analyses. The OMP table compiled by Perey in 1976 is significant and useful. It is very necessary and valuable to set up a new OMP data file, in which the OMP sets should be collected and compiled in a suitable format.

1 Two Types of OMP Sets

It will be more difficult to set up the OMP data file than others, because there are tremendous amount of information on optical model potential buried in the literature, as well as many different types of optical potentials (such as different incident particle types, local vs. nonlocal, spherical vs. deformed, different geometry shape etc.), and different types of OMP sets (such as global, regional, nucleus–specific, different E–dependence and A–dependence types of the potential parameters etc.).

In fact, there are two types of OMP sets, i. e. the global and regional OMP sets, as well as the nucleus–specific ones existing in literature. They are different in fundamental requirements and complexity of parameter sets. The former aims at maximum generality and a developing trend is adopting more complex expression, while the latter aims at maximum accuracy in reproducing the experimental data and its expression is simpler in general. For convenience of setting up data file and retrieval, we divide the OMP data into two files : the global and regional optical model parameter (GROMP) file and nucleus– specific optical model parameter (NSOMP) file, in which two types of OMP sets mentioned above are compiled respectively. They are the data files of OMP sub–library of Chinese Evaluated Nuclear Parameter Library (CENPL).

2 GROMP File

The global and regional optical model potential parameter (OMPP) sets for six types of projectiles, i. e. neutron, proton, deuteron, triton, ^{3}He and alpha are collected and compiled in parts (1) ~ (6) of the GROMP file respectively. There is a brief information table, in which the information on authors, publishing date, mass region of target nucleus, energy region of incident particle, spherical or deformed (S / D), local or nonlocal (L / N) and fitted experimental data types are included for each type of projectile. There is an entry for each set of OMPP, and each entry contains 13 subjects denoted by different keywords. They are "Entry", "Title", "Authors", "Affil.", "Ref.", "Projectile", "Nucleus Region", "Energy Region", "Potential", "Parameters", "Primary Data", "Optim. Method" and "Comments".

Up to now, the GROMP file has reached a specified scale.

3 NSOMP File

The nucleus–specific OMPP sets only for neutron projectile are collected and compiled in the NSOMP file. The brief information on each set of OMPP and its potential parameters are listed in this file. The brief information

contains target nucleus, neutron incident energy, spherical or deformed (S / D), fitted experimental data types and made model calculations, deformed parameter and standard abbreviation of reference.

A standard optical potential form for nucleus–specific optical model potential and corresponding computer format were all determined. It not only can cover most of the OMPP sets existing in the literature at present, but also is suited for future possible development tendency of OMPP.

Up to now, about 75 sets of optimum optical model parameters for neutron, which were used in the calculations of complete neutron data in CENDL–1, 2, have been compiled. This file is only in an embryonic form.

As the next step, the data files of the OMP sub–library will further be expanded and perfected.

The project supported in part by the International Atomic Energy Agency and National Natural Science Foundation of China.

CN9701148

A Data File Relative to Level Density (CENPL.NLD.LRD–2)

Huang Zhongfu
(Physics Department, Guangxi University, Nanning, Guangxi)

Su Zongdi Sun Zhengjun
(China Nuclear Data Center, CIAE)

1 Average Neutron Resonance Parameters and Cumulative Number of Low Lying Levels

The average level spacing D_0 of s–wave neutron at the neutron separation energy B_n and the cumulative number N_0 of low lying levels are the most basic data in the nuclear level density researches. The D_0, as well as the neutron strength function S_0, radiative capture width GW_0 etc. for s–wave neutron at B_n are major parameters describing the mean properties in the resonance region. It is necessary and important to estimate the reliable D_0 and N_0 values

in order to fit the accurate level density parameters. Estimation method of the D_0, including moment method, maximum likelihood method, Bayesian approach and so on, as well as corresponding program AVRPES[1] were studied and further developed for more than ten years. The N_0 values were evaluated by means of the histogram. Three sets of the D_0 and N_0 values were evaluated and recommended in 1984, 1988 and 1993 respectively. Based on these data, three sets of level density parameters for the composite four formulas of the parameters of constant temperature–Fermi gas, back–shifted Fermi gas formula and generalized superfluid model were extracted[2~4], respectively. The D_0 and N_0 values recommended by us in 1993 were included in the data file relative to the level density LRD–1 (The First Version)[5], and the three sets of level density parameters were compiled in the file of level density parameters LDP–1 (The First Version)[6]. The both of LRD and LDP are the data files of Nuclear Level Density (NLD) Sub–Library of the Chinese Evaluated Nuclear Parameter Library (CENPL).

2 Updated D_0 and N_0 Values

Recently, the program AVRPES was further refined, the resolved resonance parameters from BNL–325, ENDF / B–6, JEF–2, and JENDL–3 were collected and analysed, a set of the resolved resonance parameters were evaluated, the data of nuclear discrete levels were further supplemented and corrected according to recent data published in *Nuclear Data Sheets*. A new set of average neutron resonance parameters and N_0 values for more than 300 nuclides have been reestimated on the basis of the work mentioned above. Based on these updated data, a new LRD file, LRD–2 (Second Version) was recommended in 1996.

3 LRD–2

The LRD–2 file contains the D_0 and N_0 values of 344 nuclides, S_0 values of 309 ones ranging from ^{15}N to ^{254}Es, as well as the GW_0 values of 208 ones ranging from ^{35}S to ^{250}Bk. Most of the D_0 values (for 309 nuclides), all the S_0 and N_0 values were reevaluated in 1996[5]. The other D_0 values of 35 nuclides were taken from Refs. [7] ~ [17], the GW_0 values were taken from BNL–325[11].

Each record of this file contains the atomic number Z(I4), element symbol EL(A3), mass number A(I4), spin I(A6) of ground state for ($Z,A-1$) nucleus, neutron separation energy B_n(F7.3), neutron energy internal to deter-

mine the average level spacing E_l(E10.3), resonance number N_r(I4) in E_l, D_0(E9.2) and its deviation dD_0(E9.2), S_0(F5.2) and its deviation dS_0(E5.2), GW_0, cut off excitation energy U_m(f5.2) to get N_0 and N_0(I4).

The comparison between updated s–wave average resonance parameters D_0, S_0 and cumulative number N_0 of low levels and ones of LRD–1 data file are shown in Table 1.

Table 1 Comparison between 1993 version and 1996 version data

	1993 version	1996 version
Data	D_0, S_0, N_0	D_0, dD_0, S_0, dS_0, N_0
Nuclides	332, ^{17}O~^{254}Es (D_0 & N_0) 202, ^{24}Na~^{254}Es (S_0)	344, ^{15}N~^{254}Es (D_0 & N_0) 311, ^{15}N~^{254}Es (S_0)
Resolved Resonance Parameters	ENDF / B–6	BNL–235, ENDF / B–6 JEF–2, JENDL–3
Discrete level schemes	ENSDF (File as of 1991)	ENSDF corrected by recent < Nucl. Data Sheets > up to 1993
Methods	The moment method; maximum likelihood method Bayesian approach, etc. for D_0, The histogram of the low–lying levels, for N_0	
Program	AVRPES	

The project supported in part by the International Atomic Energy Agency.

References

[1] Huang Zhongfu, Chinese J. Atomic Energy Sci. & Tech., 22, 3(1988)

[2] Su Zongdi et al., INDC(CPR)–2, 1985

[3] Huang Zhongfu et al., Chinese J. Nucl. Phys., 13, 147(1991)

[4] Lu Guoxiong et al., to be published

[5] Huang Zhongfu et al., Four Kinds of Data Relative to Level Density, unpublished, 1993

[6] Su Zongdi et al., CNDP, 13, 129(1995)
[7] Huang Zhongfu et al., New Sets of S–Wave Average Resonance Parameters. to be published
[8] J. Kopecky et al., INDC(NDS)–238(1990)
[9] J. A. Harver et al., Phys. Rev., C28, 24(1983)
[10] W. Dilg et al., Nucl. Phys., A217, 269(1973)
[11] S. F. Mughabghab et al., Neutron Cross Section, Academic Press, Inc., Part A(1981) and Part B(1984)
[12] S. Iijima et al., J. Nucl. Sci. Tech., 21, 10(1984)
[13] S. Raman et al., Phys. Rev., C23, 2794(1981)
[14] T. Asami et al., JAERI–M 86–086 (1986)
[15] V. M. Bychkov et al., INDC(CCP)–320(1990)
[16] J. L. Cook et al., Aust. J. Phys., 20, 477(1967)
[17] G. D. James et al., Nuclear Fission and Neutron–Induced Fission Cross Sections, Oxford, Pergamon Press, 174 (1981)
[18] G. V. Antsipov et al., INDC(CCP)–239 (1989)

CINDA INDEX

Nuclide	Quantity	Energy (eV)		Lab	Type	Documentation			
		Min	Max			Ref	Vol	Page	Date
^{1}H	Total	2.0+7	2.0+10	AEP	Eval	Jour CNDP	16	49	Dec 96
^{11}B	(p,n)	Thrsh	8.0+ 7	AEP	Eval	Jour CNDP	16	58	Dec 96
^{13}C	(p,n)	Thrsh	8.0+ 7	AEP	Eval	Jour CNDP	16	58	Dec 96
^{15}N	(p,n)	Thrsh	8.0+ 7	AEP	Eval	Jour CNDP	16	58	Dec 96
^{16}O	(p,x)	Thrsh	8.0+ 7	AEP	Eval	Jour CNDP	16	58	Dec 96
^{28}Si	(n,xγ)	1.4+7		AEP	Theo	Jour CNDP	16	73	Dec 96
Ti	(n,xγ)	1.5+7		AEP	Theo	Jour CNDP	16	73	Dec 96
^{52}Cr	(p,x)	Thrsh	3.0+ 7	AEP	ExTh	Jour CNDP	16	33	Dec 96
^{89}Y	(n,xγ)	1.4+7		AEP	Theo	Jour CNDP	16	73	Dec 96
^{103}Rh	(n,x)	2.0+3	2.5+ 7	UNW	Theo	Jour CNDP	16	41	Dec 96
^{169}Tm	(n,xn)	1.4+7	1.0+ 8	AEP	Theo	Jour CNDP	16	68	Dec 96
	Calculation	1.4+7	1.0+ 8	AEP	Theo	Jour CNDP	16	28	Dec 96
^{181}Ta	(n,xγ)	5.0+6		AEP	Theo	Jour CNDP	16	73	Dec 96
W	(n,xγ)	1.7+7		AEP	Theo	Jour CNDP	16	73	Dec 96
^{193}Ir	(n,2n)	1.4+7		LNZ	Expt	Jour CNDP	16	16	Dec 96
^{197}Au	(n,xγ)	1.4+7		AEP	Theo	Jour CNDP	16	73	Dec 96
^{197}Au	Frag Angdis	?	7.0+ 7	BHU	Expt	Jour CNDP	16	5	Dec 96
^{207}Pb	Frag Angdis	?	7.0+ 7	BHU	Expt	Jour CNDP	16	5	Dec 96
^{209}Bi	Frag Angdis	?	7.0+ 7	BHU	Expt	Jour CNDP	16	5	Dec 96
^{238}U	Diff Elastic	5.0+6		AEP	Theo	Jour CNDP	16	25	Dec 96

UNW = North–Western University, Xian, China

Author, Comments
Liu Tingjin, SIG
Zhuang Youxiang, SIG, EVAL
Zhuang Youxiang, SIG, EVAL, CALC
Zhuang Youxiang, SIG, EVAL, CALC
Zhuang Youxiang, SIG–N13, EVAL, CALC
Fan Sheng+, G–SPEC, SYSTEMATICS
Fan Sheng+, G–SPEC, SYSTEMATICS
Xu Xiaoping+, SIG, CALC, EVAL
Fan Sheng+, G–SPEC, SYSTEMATICS
Sun Xiuquan+, CALC, SIG, DA, DE
Yu Baosheng+, SIG–TM 168–165
Shen Qingbiao+, SIG, CALC
Fan Sheng+, G–SPEC, SYSTEMATICS
Fan Sheng+, G–SPEC, SYSTEMATICS
Kong Xiangzhong+, SIG, TBL, ACTIV
Fan Sheng+, G–SPEC, SYSTEMATICS
Jaint, ANGDIS
Jaint, ANGDIS
Jaint, ANGDIS
Wang Shunuan, ANGDIS, ECIS95

(京)新登字 077 号

图书在版编目(CIP)数据

中国核科技报告:核数据进展通讯 1996 No. 16:英文/庄友祥等著. —北京:原子能出版社,1996
ISBN 7-5022-1626-X

Ⅰ. 中… Ⅱ. 庄… Ⅲ. 核技术-研究报告-中国-1996-英文 Ⅳ. TL-2

中国版本图书馆 CIP 数据核字 (96) 第 23072 号

原子能出版社出版发行
责任编辑:李曼莉
社址:北京市海淀区阜成路 43 号 邮政编码:100037
中国核科技报告编辑部排版
核科学技术情报研究所印刷
开本 787×1092 1/16 · 印张 5 · 字数 80 千字
1996 年 12 月北京第一版 · 1996 年 12 月北京第一次印刷

CHINA NUCLEAR SCIENCE & TECHNOLOGY REPORT

ISBN 7-5022-1626-X

9 787502 216269 >